NASA Technical Memorandum 105208

Resonant Triad in Boundary-Layer Stability
Part I. Fully Nonlinear Interaction

Reda R. Mankbadi
Lewis Research Center
Cleveland, Ohio

September 1991

NASA

RESONANT TRIAD IN BOUNDARY-LAYER STABILITY

PART I. FULLY NONLINEAR INTERACTION

Reda R. Mankbadi
National Aeronautics and Space Administration
Lewis Research Center
Cleveland, Ohio 44135

SUMMARY

A first-principles theory is developed to study the nonlinear spatial evolution of a near-resonance triad of instability waves in boundary-layer transition. This triad consists of a plane wave at fundamental frequency and a pair of symmetrical, oblique waves at the subharmonic frequency. A low-frequency, high-Reynolds-number asymptotic scaling leads to a distinct critical layer where nonlinearity first becomes important; the development of the triad's waves is determined by the critical layer's nonlinear, viscous dynamics. The resulting theory is fully nonlinear in that all nonlinearly generated oscillatory and nonoscillatory components are accounted for.

The presence of the plane wave initially causes exponential-of-exponential growth of the oblique waves. However, the plane wave continues to follow the linear theory, even when the oblique waves' amplitude attains the same order of magnitude as that of the plane wave. A fully interactive stage then comes into effect when the oblique waves exceed a certain level compared to that of the plane wave. The oblique waves react back on the fundamental, slowing its growth rate. The oblique waves' saturation results from their self-interaction - a mechanism that does not require the presence of the plane wave. The oblique waves' saturation level is independent of their initial level but decreases as the obliqueness angle increases.

Part II of this study will present results for the composite solution and comparisons with observations. Novel features of the phenomena will be described, and new interpretations of the experimental data will be given therein.

1. INTRODUCTION

1.1. Background

Experiments on boundary-layer transition and accompanying instability-wave growth have identified several distinct flow-development regimes. The first regime begins with the onset of a two-dimensional, Tollmien-Schlichting (TS) wave that propagates in the flow direction and is uniform in the spanwise direction. These waves harmlessly grow and decay in accordance with the two-dimensional, linear stability theory when their amplitudes are sufficiently small. However, a nonlinear regime characterized by a three-dimensional disturbance field appears when the amplitude becomes sufficiently large. These

three-dimensional disturbances grow at much higher rates than predicted by linear theory and ultimately lead to the transition to the turbulent state.

The occurrence and growth of three-dimensionality have been recognized as a prerequisite for the eventual transition into turbulence since the experiments of Klebanoff & Tidstrom (1959) and of Klebanoff, Tidstrom, & Sargent (1962), which demonstrated that the three-dimensional structures are periodic in the spanwise direction. These experiments, which incorporated relatively large two-dimensional input disturbances, documented the wrapping of the initial TS wave into peak-valley pairs characterized by streamwise wavelengths equal to that of the TS wave and to a spanwise wavelength of the same order. But at low-to-intermediate levels of the two-dimensional input disturbances, the experiments of Knapp & Roache (1968); Kachanov, Kozlov, & Levchenko (1978); Kachanov & Levchenko (1984); Saric & Thomas (1983); Saric, Kozlov, & Levchenko (1984); and Corke & Mangano (1987, 1989) indicated the existence of another form of the spanwise periodic structure. In these experiments, a staggered λ-shaped pattern occurred, the streamwise wavelength was twice that of the TS wave, and the spanwise wavenumber was almost half of that observed by Klebanoff *et al*. The three-dimensional structure is thus the subharmonic of the input TS wave. Unlike the TS wave, the observed subharmonic oblique waves grow rapidly and eventually lead to the transition to the turbulent state. Since this structure occurs at low-to-intermediate amplitudes of the TS wave, it is more likely to occur in natural transition than is the fundamental-type structure of Klebanoff *et al*. These experimental observations established the subharmonic route to boundary-layer transition, which is the subject of the present work.

The observed three-dimensionality in boundary-layer transition has prompted several theoretical and numerical attempts to find the mechanisms associated with the rapid development of the three-dimensional waves. Raetz (1959) and Craik (1971) suggested the existence of a resonant triad consisting of a plane wave and a pair of symmetrical oblique waves. Their studies suggested that, if the wavenumbers are such that the phase velocities are equal, then the interactions might be strong. This is attributed to the phase-coupled energy exchange among the wave components and to the possible transfer of energy from the mean flow to the waves in the critical layer. Though the proposed model could not quantitatively explain the observed phenomena, it revealed the existence of a particularly strong, nonlinear resonance mechanism for the selective growth of a pair of oblique waves and established in principle the subharmonic route to boundary-layer transition. Smith & Stewart (1987) considered the resonant interactions at wavenumbers close to the lower branch of the neutral stability curve by starting from the unsteady, triple-deck equations where the critical layer has moved into the viscous wall layer and is passive. The linear secondary stability analysis of Herbert (1983, 1988) explained many features of the observed phenomena in the parametric resonance stage. Other theoretical and numerical work on the subject is reviewed by Craik (1986); Stuart (1986); Herbert (1988); Nayfeh (1988); Fasel (1990); Saric (1990); and Kleiser & Zang (1991). These studies have resulted in considerable effort to establish the mechanisms and methods for quantitative analysis in this area.

1.2. Scope of Present Work

The present work is concerned with developing a first-principles theory for use in the study of the fully interactive, near-resonance triad in

boundary-layer transition. The triad consists of a two-dimensional TS wave at the fundamental frequency ω and of a pair of three-dimensional oblique waves at the subharmonic frequency $\omega/2$. The oblique waves make equal and opposite angles, $\pm\theta$, to the flow direction, and their common streamwise wavenumber is nearly half that of the plane wave. Observation of boundary-layer transition typically reveals harmonic time-dependent instability waves, which exhibit spatial downstream growth that is described in the early stages by linear stability theory. As such, we will here consider initially linear instability waves whose continued downstream spatial growth results in nonlinearity (as was first done by Goldstein, Durbin, & Leib, 1987). Here, the fully nonlinear interactions of the waves have been studied via matched asymptotic expansion in the nearly common, critical layer at the transverse position where the instability wave's phase velocity equals that of the mean flow.

Critical-layer nonlinearity (CLN) has been successfully adapted for the study of the nonlinear development of stability waves in various situations. Maslowe provided an excellent review of CLN in shear flows; more recently, Huerre (1987) considered the two-dimensional shear layer in the viscous, critical-layer regime where growth, or nonequilibrium, effects are negligible. Critical-layer nonlinearity in the nonequilibrium regime, where growth effects are dominant, has been considered by Goldstein & Leib (1988, 1989); Goldstein & Hultgren (1988); and Goldstein & Choi (1989), who showed that nonequilibrium (i.e., growth) effects must be accounted for in order to match the nonlinear solution onto a suitable linear instability wave in the upstream region, where the wave amplitudes are small. They used their analysis to study various phenomena in free shear flows, such as nonlinear roll-up effects, the nonlinear evolution of a single oblique wave on compressible and incompressible shear layers, the nonlinear interaction of a pair of oblique waves in a free shear layer, and the instabilities in supersonic mixing layers.

For boundary-layer flows, Goldstein, Durbin, & Leib (1987) used CLN to study the nonlinear roll-up of vorticity in the presence of adverse pressure gradients, and Goldstein & Wundrow (1990) used CLN to study nonlinear second-mode instability in high Mach-number boundary layers. The role of CLN in boundary-layer transition is evident from experimental observations, such as those of Corke & Mangano (1989), whose work demonstrates that nonlinearities are concentrated in the critical layer. The numerical results of secondary stability analysis (Herbert, 1988) also suggest that secondary instability originates from the redistribution of spanwise vorticity in the critical layer.

Subharmonic resonance experiments in boundary layers (Corke & Mangano, 1987, 1989; Kachanov & Levchenko, 1984; Saric & Thomas, 1983; and Saric *et al.*, 1984) indicate that at least three stages of the nonlinear interactions follow the initial linear growth stage: super-exponential subharmonic growth, saturation, and decay. In the super-exponential stage, or, loosely termed, the parametric resonance stage, the subharmonic oblique waves grow rapidly while the fundamental plane wave behaves almost in accordance with the linear theory. This stage is followed by the fully interactive regime, wherein the subharmonic exceeds the fundamental, saturates, and then decays. This regime, which may or may not be associated with a backreaction on the fundamental, ultimately results in the transition to the turbulent state. The recent experiments of Corke & Mangano (1989) and Corke (1989) have indicated the existence of several previously unencountered features of the fully interactive regime. Also, the fully interactive regime has not been completely explored by direct numerical

simulations owing to the resolution requirements, which become prohibitive as the amplitudes increase downstream. For these reasons, this study focuses on the nonlinear interactions of the waves, starting from the linear stage and encompassing the resonance as well as the fully interactive saturation and decay stages. Emphasis is placed on capturing the fully interactive regime, which is done by allowing the oblique waves a sufficiently large amplitude to produce a backreaction on the plane wave.

Because the above-cited experimental observations also indicate that subharmonic resonance occurs at low dimensionless frequencies, this study employs an asymptotic analysis that is valid not only in the low-frequency domain relevant to the experimentally observed phenomena but also at the technologically important lower-frequency domain, which may not be easily made subject to experimental testing or direct numerical simulations.

Subharmonic resonance first occurs near, and continues downstream of, the upper-branch neutral stability curve (see the data of Kachanov & Levchenko, 1984; Saric & Thomas, 1983; Saric, Kozlov, & Levchenko, 1984; Corke & Mangano, 1987, 1989; and §3.4, part II of this study). The parametric resonance mechanism is proportional to the plane wave's amplitude, which peaks at the upper branch; furthermore, as this study will demonstrate, the parametric resonance mechanism also is proportional to the cube of the Reynolds number, which increases indefinitely downstream. For all these experiments, these two factors cause resonance to occur in the vicinity and downstream of the upper branch, with the subharmonic maximum growth rate occurring not at, but downstream of, the upper branch. Therefore, the upper-branch scaling (Drazin & Reid, 1981) must be relevant to the subharmonic resonance phenomena.

Moreover, at low frequencies, the upper-branch scaling applies not only in the vicinity of the upper branch, but also over most of the Reynolds-number range, breaking down only at low Reynolds numbers in the asymptotically small neighborhood of the lower branch (Goldstein & Durbin, 1986). Therefore, the upper-branch scaling is relevant to the entire Reynolds-number range associated with the subharmonic resonance phenomena. This scaling leads to a multideck stability structure characterized by a distinct, nonlinear, viscous critical layer separated from the viscous wall layer, and it cannot be captured by a triple deck structure (see Bodonyi & Smith, 1981; and Drazin & Reid, 1981, and references therein).

The above factors uniquely fix the asymptotic scaling. As such, in this study a low-frequency, high-Reynolds-number scaling is adopted that is applicable to all the Reynolds-number range relevant to the observed subharmonic resonance. This scaling brings into play the critical layer and distinguishes it from the viscous wall layer.

Section 2 of this study addresses the linear solution in the main part of the boundary layer. Slowly varying amplitude functions are introduced in the linear solution and are ultimately determined by considering the nonlinear viscous flow in the critical layer for each mode. The high-Reynolds-number linear solutions are obtained by matching the appropriate results in the different transverse zones. This leads to a linear relationship between the growth rate and the velocity jump across the critical layer. The waves then interact nonlinearly, with the nonlinearity first coming into effect in the nearly common critical layer.

Section 3 addresses the nonlinear, viscous critical-layer flow. The nonlinear viscous critical layer is required to approach a conventional linear, viscous critical layer far upstream. Within the order of approximation of the analysis, nonlinear effects are confined to the critical layer, thus providing the boundary conditions required to solve the viscous nonlinear equations that govern the critical-layer flow. The scales of amplitudes are determined for the fully interactive case, which implies that the oblique waves can become large enough to cause a backreaction on the plane wave. The self-interaction of the oblique waves occurs at the same level and is found to be of major importance.

Section 4 addresses the nonlinear amplitude equations for the triad waves. The nonlinear solution presented here matches onto the upstream linear solution and onto the linear solution outside the critical layer. The amplitude equations are obtained analytically by equating the velocity jumps across the critical layer that are calculated from the linear solution to those that are calculated from the nonlinear solution.

Section 5 examines the nonlinear mechanisms independently of the flow divergence effects, which is feasible because of the comparatively short streamwise distance wherein nonlinearity occurs. Here, the study demonstrates that the saturation of the oblique waves is caused by their self-interaction, even in the absence of the plane wave. This self-interaction, which leads to the saturation and decay of the oblique waves, previously has not been identified in the subharmonic route to boundary-layer transition. The parametric resonance of the subharmonic caused by the plane wave, and the backreaction that occurs on the latter are also examined in §5. This is followed by the presentation of discussions and conclusions in §6.

Part II of this study will examine the influence exerted over the development of instability waves by flow-divergence effects. This will be achieved by following Goldstein & Leib (1988) in forming a composite solution that accounts for both the nonlinear effects and for those caused by the boundary-layer growth. The results will be compared with experimental data as well as with numerical simulations, and excellent agreement will be demonstrated.

Part II of this study also will examine other waves generated by the nonlinear interactions, waves that were not present in the initial (upstream) linear stage and which are fully accounted for in the present theory. These waves are of significant magnitude and play a crucial role in determining the triad's amplitudes as well as in interpreting several previously unexplained experimental observations.

In addition, part II will examine the broad range of unstable spanwise wavenumbers.

2. SCALING AND LINEAR SOLUTION

The flow under consideration here is that of an incompressible laminar boundary layer. Its mean boundary-layer velocity is given by the Blasius velocity U_B, where

$$U_B = \lambda y - \frac{\lambda^2}{2\cdot 4!} y^4 + \ldots \text{ as } y \to 0 \qquad (2.1)$$

and λ denotes the scaled Blasius skin friction = 0.332. The upstream flow starts as a near-resonance triad of spatially growing instability waves: a two-dimensional mode of normalized frequency ω and wavenumber α, and a pair of subharmonic oblique waves of frequency $\omega/2$, streamwise wavenumber nearly equal to $\alpha/2$, and spanwise wavenumber $\pm\beta$. The development of the waves upstream of the nonlinear region (fig. 1(a)) follows the weakly nonparallel flow linear theory. All velocities are normalized by the upstream velocity U_∞, lengths by δ^*, time by δ^*/U_∞, and pressure by ρU_∞^2, where ρ is the fluid density and δ^* is the boundary-layer thickness defined as $\delta^* = \sqrt{\nu x/U_\infty}$. Here, ν is the kinematic viscosity.

The high-Reynolds number scales as

$$\bar{R} = \sigma^{10} R \,, \qquad (2.2)$$

where R is the Reynolds number based on the local-boundary layer thickness, δ^*, and $\bar{R}$ is an order-one scaled Reynolds number and a real quantity for time-periodic spatially growing disturbance. The small-frequency parameter σ can be related to the normalized frequency F^* by the approximate relation in Goldstein & Durbin (1988)

$$F^* = \frac{\omega\nu}{U_\infty^2} = \sigma^{12} \,. \qquad (2.3)$$

The normalized complex wavenumber α is small, and its imaginary part is smaller than its real part (Goldstein, Durbin, & Leib, 1987). Consequently, each of the three modes has a well-defined critical layer at nearly the same transverse position, y_c, where the real part of their nearly common phase velocity, c, is equal to the streamwise velocity, U.

Outside the critical layer, the unsteady flow is governed by the linear dynamics, as first pointed out by Haberman (1972), and is treated as being locally parallel in the streamwise length scale over which the nonlinear effects take place. The velocity field is given by

$$u = U_B(y) + Re\left\{\varepsilon A_0(x_1)\frac{\partial \Phi_0}{\partial y}(y,x_1,\sigma)e^{iX} + \delta A(x_1)\left[U_+(y,x_1,\sigma)e^{iZ} + U_-(y,x_1,\sigma)e^{-iZ}\right]e^{iX/2}\right\} \qquad (2.4a)$$

$$v \equiv Re\, i\left[\varepsilon\alpha A_0\Phi_0 e^{iX} + \delta\gamma A(e^{iZ} + \bar{e}^{iZ})\Phi\bar{e}^{iX/2}\right] \qquad (2.4b)$$

and

$$w = \delta Re\, A\left(W_+ e^{iZ} + W_- e^{-iZ}\right)e^{iX/2} \,, \qquad (2.4c)$$

where

$$x_1 \equiv \sigma^4 x \tag{2.5a}$$

$$X \equiv \bar{\alpha}(x - \sigma\bar{c}t) \tag{2.5b}$$

$$Z \equiv \beta z \tag{2.5c}$$

$$\gamma \equiv \sqrt{\left(\frac{\alpha}{2}\right)^2 + \beta^2} \ . \tag{2.5d}$$

The amplitudes A_0 and A are for the two-dimensional and the oblique waves, respectively. The symbols ε and δ are the measures of the amplitudes of the two-dimensional and the oblique waves, respectively. The amplitude functions and their scales will ultimately be determined from the nonlinear analysis in the critical layer. Because the initial development of the instability waves is linear, we can take $A(x_1)$ to be initially a real quantity, but we allow the two-dimensional amplitude $A_0(x_1)$ to be complex. Farther downstream, because of the nonlinear effects, both $A(x_1)$ and $A_0(x_1)$ become complex. In (2.4), $U_\pm$ and $W_\pm$ are related to the eigenfunction Φ through the relations

$$\frac{\sqrt{\gamma^2 - \beta^2}}{\gamma} U_\pm \pm \frac{\beta}{\gamma} W_\pm = \frac{\partial \Phi}{\partial y} \tag{2.6a}$$

$$\frac{\beta}{\gamma} U_\pm \mp \frac{\sqrt{\gamma^2 - \beta^2}}{\gamma} W_\pm = \frac{\beta U'}{\sqrt{\gamma^2 - \beta^2}} \frac{\Phi}{U - c} \ , \tag{2.6b}$$

where Φ_0, Φ satisfy the linear Orr-Sommerfeld and Squire equations, respectively, with appropriate boundary conditions. The wavenumbers and phase velocities scale as (see Goldstein, Durbin, & Leib, 1987)

$$\alpha = \sigma\bar{\alpha} + \sigma^4 \frac{A_0'}{iA_0} \ , \tag{2.7a}$$

$$\gamma = \sigma\bar{\gamma} + \frac{\sigma^4}{2i} \frac{\bar{\alpha}}{\bar{\gamma}} \frac{A'}{A} \ , \tag{2.7b}$$

$$c_0 = \frac{\sigma\bar{c}}{1 + \dfrac{\sigma^3}{i\bar{\alpha}} \dfrac{A'}{A_0}} \ , \tag{2.7c}$$

$$c = \frac{\sigma\bar{c}}{1 + 2\dfrac{\sigma^3}{i\bar{\alpha}} \dfrac{A'}{A}} \ , \tag{2.7d}$$

and

$$\bar{c} = \frac{\bar{R}}{\bar{\alpha}} , \tag{2.7e}$$

where an overbar ($^-$) denotes an order-one real constant. Here, ($'$) denotes differentiation with respect to the flow variable x_1. The scaling, given by equations (2.1) and (2.7), is consistent with Reid's (1965) equation (3.128).

At the high-Reynolds-number limit, the disturbance solution is a multi-zoned structure (fig. 1(b)), wherein the critical layer is distinct from the wall layer (see Bodonyi & Smith, 1981; Drazin & Reid, 1981; Graebel, 1966; Eagles, 1969; Fraenkel, 1969; and DeVillers, 1975). Zone I (Stokes layer) is a viscous wall layer and is the zone closest to the wall. Zone II (Tollmien region) is an inviscid rotational zone of adjustment within which the critical layer III is induced. Zone IV is above zone II and is an inviscid rotational region comprising most of the boundary layer. Above zone IV is the quasisteady zone V, in which the flow properties are of an inviscid irrotational type, $U = 1$, $V = 0$. Zones IV and V can be combined into one zone (Heisenberg region).

The linear solutions in the above zones are presented in appendix A. Matching the inner solutions in zones II and IV produces relations (A.4.8) to (A.4.11), which below are written for the lowest order of approximation as

$$\bar{\gamma} = \bar{\alpha} , \tag{2.8a}$$

$$\lambda \frac{\bar{c}}{\bar{\alpha}} = 1 , \tag{2.8b}$$

$$\left(\cos\theta + \frac{1}{\cos\theta}\right)\frac{A'}{A} = \frac{\left(\bar{\gamma}\bar{c}\right)^2}{4\lambda^3}(\Delta\phi) + \frac{\bar{\gamma}^2}{(\bar{c})^2\sqrt{2\bar{c}R\bar{\gamma}}} , \tag{2.9a}$$

$$\frac{A_o'}{A_o} = \frac{\left(\bar{\alpha}\bar{c}_o\right)^2}{8\lambda^3}(\Delta\phi_o) + \frac{\bar{\alpha}^2}{2(\bar{c}_o)^2\sqrt{2\bar{c}_o\bar{R}\bar{\alpha}}} + i\,\mathrm{Im}\left(\frac{A_o'}{A_o}\right)_{\text{initial}} . \tag{2.9b}$$

Here, y_c is the location of the critical layer, which scales as

$$y_c = \sigma Y_c , \tag{2.10}$$

where Y_c is an order-one real constant and $\Delta\phi$ and $\Delta\phi_o$ are the velocity jumps across the critical layer for the oblique and two-dimensional modes, respectively. The obliqueness angle, θ, is given by

$$\theta = \sin^{-1}\frac{\bar{\beta}}{\bar{\gamma}} . \tag{2.11a}$$

Upon substituting relations (2.5d) and (2.8a) into relation (2.11a), we obtain

$$\theta = 60^{\circ} \ . \tag{2.11b}$$

The velocity field in zone II, which contains the critical layer, is given according to the linear solution (appendix A) as

$$u = \sigma\lambda Y - \sigma^4 \frac{Y^2}{2}\left(\frac{\lambda^2}{4!} Y^2\right) + Re\left\{\left[\lambda + \sigma a_o + \sigma^3\left(f' + i\mu_c Y_c \phi_o^{\pm}\right)\right]\varepsilon A_o e^{iX} + 2\left(\frac{\lambda + \sigma a}{\cos\theta}\right.\right.$$

$$+ \frac{\bar{c}(\lambda + \sigma a)}{\lambda Y - \bar{c}} \tan\theta \sin\theta + \sigma^3\left\{f' \cos\theta + \frac{\tan\theta \sin\theta}{\lambda Y - \bar{c}}\left\{\lambda F(o) + \mu_c \bar{c}\right.\right.$$

$$\times \left[(Y - Y_c)\ln|Y - Y_c| + Y_c \ln Y_c\right] + \lambda Y^2\left[\frac{1}{2}\mu_c - \frac{\lambda^2 Y}{4!}\left(Y_c + \frac{5}{2} Y\right.\right.$$

$$\left.\left.\left.\left. - \frac{\lambda}{\lambda Y - \bar{c}} \frac{Y^2}{2}\right)\right]\right\} + \frac{\lambda A'}{\bar{\gamma} i A} \sin^2\theta\left[1 - \frac{\lambda Y}{\lambda Y - \bar{c}}\left(1 + \frac{\lambda Y}{\lambda Y - \bar{c}} \frac{1}{\cos^2\theta}\right)\right]$$

$$\left.\left.\left. + \frac{i\mu_c Y_c}{\cos\theta}\left(\phi^{\pm} + \frac{\bar{c}}{\lambda Y - \bar{c}} \phi^{-} \sin^2\theta\right)\right)\right)(\cos Z)\delta A e^{iX/2}\right\} + \ldots , \tag{2.12a}$$

$$v = -\sigma^2 \lambda Y \, Re\left[i\bar{\alpha}\varepsilon A_o e^{iX} + 2i\bar{\gamma}(\cos Z)\delta A e^{iX/2}\right] + \ldots , \tag{2.12b}$$

$$w = -2\delta(\sin\theta \sin Z) \, Re \, \frac{\bar{c}\lambda}{\lambda Y - \bar{c}} \, iA e^{iX/2} + \ldots , \tag{2.12c}$$

$$p = \sigma\bar{c}\lambda \, Re\left[\varepsilon A_o e^{iX} + 2(\cos\theta \cos Z)\delta A e^{iX/2}\right] + \ldots , \tag{2.12d}$$

where

$$f' = \mu_c\left(Y + Y_c \ln|Y - Y_c| + Y_c\right) - \frac{\lambda^2}{2} Y^2\left(\frac{Y_c}{4} + \frac{Y}{3!}\right) \tag{2.12e}$$

and

$$\mu_c = -\frac{\lambda^2 Y_c^2}{4} \ . \tag{2.12f}$$

3. FULLY INTERACTIVE NONLINEAR SOLUTION IN CRITICAL LAYER

The previous linear solution, (eq. (2.12)), becomes singular at the critical layer. The appropriate transverse scaling coordinate in this region, which matches to the linear growth rate, is given by

$$\bar{\eta} = \frac{Y - Y_c}{\sigma^2} \quad . \tag{3.1}$$

This scaling of the critical-layer thickness also is consistent with Reid's (1965) result that the critical layer has a thickness on the order of $(\alpha R)^{-1/3}$. Then, on substituting (3.1) into (2.12), the critical layer solution expands as follows

$$u - c = \sigma^3\lambda\bar{\eta} + \sigma^6\mu_c^+ Y_c\bar{\eta} + \sigma^8\mu_c \frac{1}{2}\bar{\eta}^2 + \delta\sigma^{-2}u_{-2} + \delta\sigma^{-1}u_{-1} + \delta u_0 + \delta\sigma u_1 + \delta\sigma^2 u_2$$

$$+ \delta\sigma^3 u_3 + \varepsilon u_0^{(o)} + \varepsilon\sigma u_1^{(o)} + \varepsilon\sigma^2 u_2^{(o)} + \varepsilon\sigma^3 u_3^{(o)} + \ldots , \tag{3.2a}$$

$$\bar{v} = -\varepsilon\sigma^{-2}\bar{\alpha}\lambda Y_c \, Re \; iA_o e^{iX} - \delta\sigma^{-2}\bar{\gamma}\lambda Y_c \; 2\cos Z \, Re \; iAe^{ix/2} + \ldots , \tag{3.2b}$$

$$w = \delta\sigma^{-2}w_{-2} + \delta\sigma^{-1}w_{-1} + \delta w_0 + \delta\sigma w_1 + \delta\sigma^2 w_2 + \delta\sigma^3 w_3 + \ldots , \tag{3.2c}$$

$$p = \varepsilon\sigma\bar{c}\lambda \, Re \; A_o e^{iX} + \delta\sigma\bar{c}\lambda \cos\Theta \; 2\cos Z \, Re \; Ae^{iX/2} + \ldots . \tag{3.2d}$$

Here, u and $u^{(o)}$ denote the oblique and plane waves, respectively, and we have written

$$v \equiv \sigma^4\bar{v} \tag{3.3a}$$

and

$$\mu_c^+ \equiv -\frac{1}{3}\left(\frac{\lambda Y_c}{2}\right)^2 \quad . \tag{3.3b}$$

The full momentum equations can be expressed in terms of the scaled variables x_1, X, Z, and $\bar{\eta}$ as

$$D\underset{\sim}{u} = -\left(\bar{\alpha}P_X + \sigma^3 P_{x_1}, \; \sigma^{-8}P_{\bar{\eta}}, \; \bar{\beta}P_Z\right) \tag{3.4a}$$

and the continuity equation as

$$\bar{\alpha}u_X + \bar{v}_{\bar{\eta}} + \bar{\beta}w_Z + \sigma^3 u_{x_1} = 0 \; , \tag{3.4b}$$

where

$$\underset{\sim}{u} \equiv (u,\bar{v},w) \tag{3.4c}$$

and

$$\bar{D} \equiv \bar{\alpha}(u - c)\frac{\partial}{\partial \bar{X}} + \bar{v}\frac{\partial}{\partial \bar{\eta}} + \sigma^3 u\frac{\partial}{\partial x_1} + \bar{\beta}w\frac{\partial}{\partial Z} - \frac{\sigma^3}{\bar{R}}\frac{\partial^2}{\partial \bar{\eta}^2} . \tag{3.4d}$$

It also is convenient to work with the equation for Z-component vorticity ω, which can be written as

$$\sigma\bar{D}\omega = \bar{\beta}\left(\sigma^{-2}u_Z w_{\bar{\eta}} + \sigma\omega w_Z - \sigma^6\bar{\alpha}\bar{v}_Z w_X - \sigma^9\bar{v}_Z w_{x_1}\right) . \tag{3.5}$$

The nonlinear terms in the critical layer solution will balance the velocity jump at the same order as in the linear solution when

$$\varepsilon = \sigma^{10} . \tag{3.6}$$

The expansion (3.2) indicates that the first order of interaction occurs when $\delta \approx \varepsilon$. This leads to a double exponential growth for the oblique waves, but the backreaction on the plane fundamental cancels out for this scaling level. The emphasis here, however, is on the fully interactive oblique and plane waves.

The next order of interaction that produces a nonzero backreaction is

$$\delta = \frac{\varepsilon}{\sigma^{2.5}} = \sigma^{7.5} . \tag{3.7}$$

This also is the same order at which the oblique wave's self-interaction appears. Substituting (3.6) and (3.7) into (3.2), the expansions are now rewritten in the general form as

$$u - \sigma\bar{c} = \sigma^3\lambda\bar{\eta} + \sigma^{5.5}U_{5.5} + \sigma^6 U_6 + \sigma^{6.5}U_{6.5} + \ldots \tag{3.8a}$$

$$w = \sigma^{5.5}W_{5.5} + \sigma^6 W_6 + \sigma^{6.5}W_{6.5} + \sigma^7 W_7 + \ldots \tag{3.8b}$$

$$\bar{v} = \sigma^{5.5}V_{5.5} + \sigma^6 V_6 + \sigma^{6.5}V_{6.5} + \sigma^7 V_7 + \ldots \tag{3.8c}$$

$$p = \sigma^{8.5}P_{8.5} + \sigma^9 P_9 + \sigma^{9.5}P_{9.5} + \sigma^{10}P_{10} + \ldots \tag{3.8d}$$

and the vorticity, ω, is given by

$$-\omega = \lambda + \sigma^{2.5}U_{5.5,\bar{\eta}} + \sigma^3 U_{6,\bar{\eta}} + \sigma^{3.5}U_{6.5,\bar{\eta}} + \sigma^4 U_{7,\bar{\eta}} + \ldots . \tag{3.8e}$$

The mean flow components at the order σ^6 and σ^8 are given by

$$\bar{u}_6 = \mu_c^+ Y_c \bar{\eta}, \tag{3.9a}$$

$$\bar{u}_8 = \mu_c \frac{\bar{\eta}^2}{2} . \tag{3.9b}$$

The linear solution indicates that

$$V_{5.5} = -\bar{c}\ Re\ 2i\bar{\gamma} \cos z\ Ae^{iX/2} , \tag{3.10a}$$

$$P_{8.5} = \lambda\bar{c}\ Re\ 2 \cos\theta \cos z\ Ae^{iX/2} , \tag{3.10b}$$

$$v_8^o = -\bar{c}\ Re\ i\bar{\alpha}A_o e^{iX} , \tag{3.10c}$$

$$P_{11}^o = \lambda\bar{c}\ Re\ A_o\ e^{iX} . \tag{3.10d}$$

Substituting (3.8) into (3.4), we obtain the nonlinear viscous equations for each term in the expansion

$$L_3 U_\ell = -\sum_{k=4} L_k U_{(3+\ell-k)} - \bar{\alpha} P_{(3+\ell),X} - P_{\ell,x_1} , \tag{3.11a}$$

$$L_3 W_\ell = -\sum_{k=4} L_k W_{(3+\ell-k)} - \bar{\beta} P_{(3+\ell),Z} , \tag{3.11b}$$

$$\frac{\partial V_\ell}{\partial \bar{\eta}} = -\left(\bar{\alpha} \frac{\partial U_\ell}{\partial X} + \bar{\beta} \frac{\partial W_\ell}{\partial Z} + \bar{c} \frac{U_{\ell-3}}{\partial x_1} \right) , \tag{3.11c}$$

where

$$L_3 = \bar{\alpha} U_3 \frac{\partial}{\partial x} - \frac{1}{\bar{R}} \frac{\partial^2}{\partial \bar{\eta}^2} , \tag{3.11d}$$

$$L_4 = \bar{c} \frac{\partial}{\partial x_1} , \tag{3.11e}$$

$$L_k = \bar{\alpha} U_k \frac{\partial}{\partial X} + V_k \frac{\partial}{\partial \bar{\eta}} + \bar{\beta} W_k \frac{\partial}{\partial Z} + U_{k-3} \frac{\partial}{\partial x_1} , \tag{3.11f}$$

$$K = \frac{11}{2}, \frac{12}{2}, \frac{13}{2}, \ldots ,$$

$$U_3 = \lambda\bar{\eta} , \tag{3.11g}$$

$$U_k = V_k = W_k = 0 \qquad \text{for} \qquad K = \frac{7}{2}, \frac{8}{2}, \frac{9}{2}, \text{ and } \frac{10}{2} . \tag{3.11h}$$

4. AMPLITUDE EQUATIONS

In order for the nonlinear and linear solutions to match, the amplitude equations must be derived by equating the velocity jump across the critical layer obtained analytically from the nonlinear solution to that obtained from the linear one. The solutions at different levels in the expansion (3.8) are needed to arrive at this result. The procedure is outlined in this section, and the details of the intermediate steps appear in appendixes B, C, and D. The interaction mechanisms contributing to the amplitude equation appear in appendix E. The amplitudes for the triad waves appear here. Other nonlinearly generated waves, which determine the velocity jump calculated from the nonlinear solution and thus contribute to the amplitude equations of the triad, appear in appendixes B and D. These nonlinearly generated waves play a key role in interpreting several experimental observations. as will be discussed in part II of this study.

4.1. Oblique Waves' Amplitude Equation

As earlier noted, the amplitude equation for the oblique wave is obtained here by equating the velocity jump from the nonlinear solution with that from the linear solution (2.9a). Examination of the expansion (3.8) and the linear solution (2.12) indicates that the velocity jump occurs at the $U_{10.5}$ level. The equation for $U^{+}_{10.5,\bar{\eta}}$ can be obtained from (3.11) as

$$L_3 U^{+}_{10.5,\bar{\eta}} = \lambda D^{+} W_{10.5} - \sum_{k=4} \Big[L_k U^{+}_{(13.5-k),\bar{\eta}} + \sin\theta\, L_{k,\eta} W_{(13.5-k)},$$

$$- \bar{\beta} \cos\theta \Big(U_{k,z} W_{(13.5-k),\bar{\eta}} - U_{k,\bar{\eta}} W_{(13.5-k),z} \Big) \Big] , \tag{4.1a}$$

where

$$U^{+} = U \cos\theta + W \sin\theta , \tag{4.1b}$$

$$D^{+} = \cos\theta\, \bar{\beta} \frac{\partial}{\partial Z} - \sin\theta\, \bar{\alpha} \frac{\partial}{\partial X} . \tag{4.1c}$$

The solution for $U^{+}_{10.5,\bar{\eta}}$ can be written in the general form

$$U^{+}_{10.5,\bar{\eta}} = Re \sum_{n=0,m=1} Q^{(nm)}_{10.5}\left(\bar{\eta},x_1\right)e^{i[(n/2)X+mZ]} \quad . \tag{4.2}$$

Our purpose here is to match the velocity jump across the critical layer obtained from the nonlinear solution to that obtained from the linear solution. Since the latter is composed only of the oblique waves $\sim\exp\left[i\left(\frac{X}{2}\pm Z\right)\right]$, the solution of $U^{+}_{10.5,\bar{\eta}}$ corresponding to $n = 1$, $m = 1$ is therefore needed. Analysis of the $U^{+}_{\ell,\bar{\eta}}$ equations indicates that $U^{+}_{\ell,\bar{\eta}}$ has no $nm = 11$ component for $\ell = 5.5$, 6.5, 7.5, 8.5, and 9.5. Thus, we can write

$$L_3U^{+(11)}_{10.5,\bar{\eta}} = \Big[U_{5.5,\bar{\eta}}D^{+}W_8 + U_{8,\bar{\eta}}D^{+}W_{5.5} - \bar{\alpha}U_{5.5}U^{+}_{8,\bar{\eta}X} - \bar{\alpha}U_8U^{+}_{5.5,\bar{\eta}X} - \bar{\beta}\left(W_{5.5}U^{+}_{8,Z}\right)_{\bar{\eta}}$$

$$- \bar{\beta}\left(W_8U^{+}_{5.5,Z}\right)_{\bar{\eta}} - V_{5.5}U^{+}_{8,\bar{\eta}\bar{\eta}} - V_8U^{+}_{5.5,\bar{\eta}\bar{\eta}}\Big]^{(11)} \quad . \tag{4.3}$$

To obtain $Q^{(11)}_{10.5}$ from the above equation, the solutions at the 5.5 and 8 levels must first be obtained. Using (3.11), the solution at the 5.5 level can be written as

$$U_{5.5} = 2\tan\Theta\cos Z\, Re\left[iQ\left(\bar{\eta},x_1\right)e^{iX/2}\right] \tag{4.4a}$$

$$W_{5.5} = 2\sin Z\, Re\left[Q\left(\bar{\eta},x_1\right)e^{iX/2}\right] \quad , \tag{4.4b}$$

where Q satisfies

$$\bar{L}_1Q = \bar{\gamma}\bar{\lambda}\bar{c}A\sin\Theta\cos\Theta \quad , \tag{4.4c}$$

and using Fourier transform, we obtain as

$$Q = A\sin\Theta\int_{-\infty}^{0} e^{iK\eta}\, e^{hK^3/3}\, dK \quad , \tag{4.4d}$$

where

$$\eta = \frac{\bar{\eta}}{\bar{c}} \tag{4.5a}$$

$$h = \frac{1}{\frac{\bar{\alpha}}{2}\lambda\bar{c}^3\bar{R}} \tag{4.5b}$$

$$\bar{x} = x_1 - x_0 \tag{4.5c}$$

and x_0 is the origin of the nonlinear region.

The solutions for the 5.5- and 8-level components, provided in appendix B, are substituted into equation (4.3) to obtain $Q_{10.5}^{(11)}$ and its Fourier transform $\hat{Q}_{10.5}^{(11)}$ (K). The velocity jump for the three-dimensional wave, J_{3D}, is given by

$$J_{3D} = \int_{-\infty}^{\infty} Q_{10.5}^{(11)}\, d\eta = \hat{Q}_{10.5}^{(11)}\ (K = 0)\ . \tag{4.6}$$

Details of the procedure are given in appendix C and the final result is

$$J_{3D} = -\frac{i\pi A}{4}\frac{\bar{R}}{\lambda^2} - \frac{3}{4}\pi\bar{R}^2\, A_o A^* + M\frac{\bar{R}^{3.5}}{\sqrt{\lambda}}A^2A^*, \tag{4.7a}$$

$$M = 1.055 - 17.8\ i\ . \tag{4.7b}$$

The jump condition as given by equation (2.9a) is now written as

$$\left(\cos\theta + \frac{1}{\cos\theta}\right)\frac{dA}{d\bar{x}} = \frac{\lambda^2}{\sqrt{2}}\frac{A}{\bar{R}} - i\,\frac{\bar{R}}{\lambda}\,J_{3D}\ . \tag{4.8}$$

Substituting (4.7) into (4.8), we obtain the amplitude equation

$$\left(\cos\theta + \frac{1}{\cos\theta}\right)\frac{dA}{dx} = \left(\frac{\lambda^2}{\sqrt{2}\,\bar{R}} - \frac{\pi}{4}\frac{\bar{R}^2}{\lambda^3}\right)A + \frac{3}{4}\pi\frac{\bar{R}^3}{\lambda}\,iA^*A_o - iM\frac{\bar{R}^{4.5}}{\lambda\sqrt{\lambda}}A^2A^*\ , \tag{4.9}$$

which for $\theta = 60°$ reduces to

$$\frac{dA}{dx} = \underbrace{\frac{4}{5}k_oA}_{\text{Linear}} + \underbrace{\frac{3}{10}\pi\frac{\bar{R}^3}{\lambda}\,iA^*A_o}_{\text{Resonance}} - \underbrace{\frac{2}{5}\,iM\frac{\bar{R}^{4.5}}{\lambda\sqrt{\lambda}}A^2A^*}_{\substack{\text{Self-}\\ \text{interaction}}}\ , \tag{4.10}$$

where

$$k_o = \frac{\lambda^2}{2\sqrt{2}\,\bar{R}} - \frac{\pi}{8}\frac{\bar{R}^2}{\lambda^3} \tag{4.11}$$

is the linear growth rate.

4.2. The Two-Dimensional Wave's Amplitude Equation

Comparing the expansion (3.8) to the linear solution (2.12) indicates that the velocity jump for the two-dimensional wave occurs at U_{13}. The equation for U_{13} is written from equation (3.11) as

$$L_3 U^+_{13\bar{\eta}} = \lambda D^+ W_{13} - \sum_{k=4} \Big[L_k U^+_{(16-k),\bar{\eta}} + \sin\theta\, L_{k,\bar{\eta}} W_{(16-k)} - \bar{\beta}\cos\theta \Big(U_{k,z} W_{(16-k),\bar{\eta}} - U_{k,\bar{\eta}} W_{(16-k),z} \Big) \Big] , \tag{4.12}$$

which reduces to

$$\begin{aligned} L_3 U^+_{13,\bar{\eta}} = \lambda D^+ W_{13} &- \Big(L_{5.5} U^+_{10.5,\bar{\eta}} + L_8 U^+_{8,\bar{\eta}} + L_{10.5} U^+_{5.5,\bar{\eta}} \Big) \\ &- \sin\theta \Big(L_{5.5,\bar{\eta}} W_{10.5} + L_{8,\bar{\eta}} W_8 + L_{10.5,\bar{\eta}} W_{5.5} \Big) \\ &+ \bar{\beta}\cos\theta \Big(U_{5.5,\bar{\eta}} W_{10.5,z} + U_{8,\bar{\eta}} W_{8,z} + U_{10.5,\bar{\eta}} W_{5.5,z} \\ &- U_{5.5,z} W_{10.5,\bar{\eta}} - U_{8,z} W_{8,\bar{\eta}} - U_{10.5,z} W_{5.5,\bar{\eta}} \Big) . \end{aligned} \tag{4.13}$$

Terms representing the interactions between components 6.5 and 9.5, 7.5 and 8.5, or 6 and 10 would have produced an interaction term proportional to A^2. However, they failed to produce a velocity jump across the critical layer and as such are not written explicitly in equation (4.13). (Goldstein & Lee, 1991, observed the same phenomenon for the case of a triad of waves in an adverse-pressure-gradient boundary layer.) Equation (4.13) provides a general solution in the form

$$U^+_{13,\bar{\eta}} = Re \sum_{n=0,m=1} Q^{(nm)}_{13}(\bar{\eta}, x_1) e^{i[(n/2)X + mz]} . \tag{4.14}$$

The linear solution at this level indicates that only the plane wave is discontinuous. Therefore, to match the nonlinear velocity jump to the linear one, only the plane-wave component $Q^{(20)}_{13}$ is needed. The procedure is similar to that outlined in §4.1; however, here the 5.5- and 8-, and 10.5-level terms are

needed to calculate $Q_{13}^{(20)}$. The jump for the two-dimensional wave, J_{2D}, is then given by

$$J_{2D} = \int_0^\infty Q_{13}^{(20)}\, d\eta = \hat{Q}_{13}^{(20)}(K = 0) \ . \tag{4.15}$$

Details of the procedure are supplied in appendix D, which gives

$$J_{2D} = -\frac{\pi i}{8}\frac{\bar{R}}{\lambda^2} A_o + M_1 \bar{R}^{3.5} \frac{A_o A^* A}{\sqrt{\lambda}} + M_2 \frac{\bar{R}^5}{\lambda} A^* A^3 \ , \tag{4.16}$$

where

$$M_1 = 0.5848 \ , \tag{4.17a}$$

$$M_2 = -0.241 \ . \tag{4.17b}$$

The jump condition (2.9b) can be written as

$$\frac{dA_o}{d\bar{x}} = \frac{\lambda^2}{2\sqrt{2}\,\bar{R}} A_o - \frac{i\bar{R}}{\lambda} J_{2D} + iA_o\, Im\left(\frac{A_o'}{A_o}\right)_{initial} \ . \tag{4.18}$$

Substituting (4.16) into (4.18), we obtain the plane-wave amplitude equation as

$$\frac{dA_o}{d\bar{x}} = \underbrace{(k_o + ik_i)A_o}_{\text{Linear}} + \underbrace{iM_1 \frac{\bar{R}^{4.5}}{\lambda\sqrt{\lambda}} A_o A A^*}_{\text{Mutual}} - \underbrace{iM_2 \frac{\bar{R}^6}{\lambda^2} A^* A^3}_{\text{Backreaction}} \ , \tag{4.19}$$

where k_i is the initial detuning factor. Equations (4.10) and (4.19) represent the amplitude equations for the oblique and plane modes, respectively. The interaction mechanisms contributing to these equations are discussed in appendix E. Equations (4.10) to (4.19) indicate that the oblique subharmonic waves at $\theta = 60°$ and the plane fundamental wave both reach the corresponding linear upper-branch neutral stability curve at $\bar{R} = 0.1537$, which is obtained by setting the linear growth rate k_o in equation (4.11) equal to zero.

5. NONLINEAR MECHANISM

Wave development is governed in part by the nonlinear dynamics considered above and by flow-divergence effects. Here, we will examine nonlinear mechanisms that occur over relatively short streamwise length scales where nonparallel effects are unimportant. The flow-divergence effects will be considered in part II, wherein a composite expansion will be obtined.

5.1. Oblique Wave Development in the Absence of the Plane Wave

Because of the significance of oblique waves to boundary-layer transition, some experiments have attempted to examine oblique-wave development in the absence of the plane wave (e.g., Robey, 1987 and Schneider, 1989). This study examines the solution of the oblique waves' amplitude equation (4.9) in the absence of the plane wave. Under such conditions, the restriction on the spanwise wavenumber dictated by equation (2.8a) is lifted, hence the obliqueness angle can take any value. According to the asymptotic linear theory, the phase speed increases with the obliqueness angle and is given by

$$\bar{c} = \sqrt{\frac{\bar{R}}{\lambda(2\cos\theta)}} \ . \tag{5.1a}$$

For a general obliqueness angle, and with no plane wave present, equation (4.9) takes the form

$$\left(\cos\theta + \frac{1}{\cos\theta}\right)\frac{A'}{A} = \left[\frac{\lambda^2}{\sqrt{2}}\,\bar{R}\,\sqrt{2\cos\theta} - \frac{\pi}{4}\frac{\bar{R}^2}{\lambda^3(2\cos\theta)}\right]A - iM(\theta)\,\frac{\bar{R}^{4.5}}{\lambda\sqrt{\lambda}}\,A^2A^* \ . \tag{5.1b}$$

This equation is solved analytically to obtain

$$A = A_i\, e^{q\,k_{ob}\bar{x}}\, G^{1+iC_\psi} \ , \tag{5.2}$$

which gives the modulus as

$$|A| = A_i\, e^{q\,k_{ob}\bar{x}}\, G \tag{5.3}$$

and the phase angle $\tilde{\psi}$ as

$$\tilde{\psi} = C_\psi\, \ell n\, G \ . \tag{5.4}$$

The initial real amplitude at $\bar{x} = 0$ is A_i, and G is the nonlinear function given by

$$G = \left(1 + d_1A_i^2 - d_1A_i^2\, e^{2q\,k_{ob}\bar{x}}\right)^{-0.5} \ , \tag{5.5}$$

where

$$d_1 = \frac{M_i \bar{R}^{4.5}}{\lambda \sqrt{\lambda}\, k_{ob}} , \tag{5.6a}$$

and the linear growth rate is given by

$$k_{ob} = \frac{\lambda^2 \sqrt{\cos \delta\theta}}{\sqrt{\bar{R}}} - \frac{\pi}{q} \frac{\bar{R}^2}{\lambda^3 \cos \theta} , \tag{5.6b}$$

$$q = \frac{1}{\cos \theta + 1/\cos \theta} , \tag{5.6c}$$

$$C_\psi = - \frac{\text{Real}(M)}{\text{Imaginary}(M)} . \tag{5.6d}$$

The case of $\theta = 60°$, relevant to the exact resonance case to be presented in part II, is discussed below. The effect of the obliqueness angle, corresponding to various spanwise wavenumbers, is discussed in §5.1(b).

5.1(a). Oblique Waves Self-Interactions at $\theta = 60°$

The self-interaction of the oblique waves at $\theta = 60°$ with no plane wave present is examined here. Equation (5.2) shows that there are only two parameters controlling the oblique-wave development. The first is the oblique waves' amplitude, A_i, and the second is the scaled Reynolds number $\bar{R}$.

Figure 2 shows the modulus of the oblique waves' amplitude for several initial values, A_i. The location with respect to the upper branch is given by $\bar{R}/\bar{R}_{up} = 0.80$, where $\bar{R}_{up} = 0.1537$ is the scaled Reynolds number at the upper-branch neutral stability curve. The initial growth depicted in figure 2 is linear. It is followed by the oblique waves' nonlinear self-interaction, a mechanism that reduces their growth rate. Next, the amplitude of the oblique waves reaches an asymptotic saturation level independent of its initial level. This saturation level can be obtained from equation (5.3) as

$$\underset{\bar{x} \to -\infty}{|A|} = \left(\frac{\lambda \sqrt{\lambda}\, k_{ob}}{M_i \bar{R}^{4.5}} \right)^{0.5} . \tag{5.7}$$

Because the waves' self-interaction in equation (5.1) is proportional to their amplitudes cubed, a higher initial amplitude is associated with a quickening of nonlinear damping effects, which causes the asymptotic saturation level of the amplitude in the nonlinear region to be independent of the initial level.

In the case of linear growth, the amplitude of the oblique waves remains real and its phase angle remains zero as initially prescribed. However, as figure 3 illustrates, nonlinearity causes the amplitude to become complex and

the phase angle to change with $\bar{x}$. Increasing the initial level of amplitude for the oblique waves causes stronger nonlinear effects and rapid changes in the phase angle. In the limit of $\bar{x} \to \infty$, the phase angle decreases linearly with $\bar{x}$ at a constant rate independent of A_i,

$$\left.\frac{d\tilde{\psi}}{d\bar{x}}\right|_{\bar{x}\to\infty} = -\frac{4}{5} C_\psi k_{ob} \,. \tag{5.8}$$

As earlier stated, the other factor controlling the self-interaction is the scaled Reynolds number. Figure 4 shows the linear and nonlinear solutions for two values of $\bar{R}$ corresponding to $\bar{R}/\bar{R}_{up} = 0.5$ and 0.95. At the smaller value of $\bar{R}$, the linear growth rate is high and causes large amplitudes. Since the nonlinearity is proportional to A^3, it produces a dramatic reduction in the amplitude. If $\bar{R}/\bar{R}_{up} = 0.95$, the linear growth rate is weak, resulting in low amplitudes and less significant nonlinear effects. The net outcome is that the saturation level of the oblique waves slowly decreases with the Reynolds number, in accordance with equation (5.7). In reality, the Reynolds number is not frozen, as assumed here, but increases in the streamwise direction owing to the boundary-layer growth. Thus, the decrease of the saturation level with the Reynolds number (fig. 4) indicates that the oblique waves' peak is followed by decay because the Reynolds number increases in the downstream direction. The oblique waves' self-interaction thus not only causes their saturation, but ultimately also their decay.

5.1(b). Effect of Obliqueness Angle

The development of the oblique waves amplitude at various obliqueness angles corresponding to various spanwise wavenumbers is shown in figure 5. The initial conditions are $\bar{R}/\bar{R}_{up} = 0.8$ and $A_i = 0.1$. Figure 5 depicts a linear growth region, followed by a nonlinear saturation region. The linear growth rate decreases with the increase of the obliqueness angle, as can be predicted from Squire's transformation. For all obliqueness angles, the self-interaction of the oblique waves leads to their saturation and ultimately to their decay.

Of particular interest are the small-angle oblique waves, which are almost as probable as is the plane wave in a real flow with natural three dimensionality. Figure 5 demonstrates that, at small angles, the linear growth is almost the same as that of the plane wave. Nonlinear effects are absent for the exact plane wave, $\theta = 0°$. But a small obliqueness angle results in pronounced nonlinear effects. The oblique waves are characterized by a three-dimensional vorticity field; therefore, the nonlinear effects appear at a lower amplitude level for the oblique waves than they do for the corresponding two-dimensional waves. Thus, for the present amplitude level, self-interaction is evident among the small-angle oblique waves but absent for the exact plane wave, $\theta = 0°$. This phenomenon is further depicted in figure 6, which shows the oblique waves' saturation level at $\bar{x} = 100$ versus the obliqueness angle. An abrupt drop in the saturation level is apparent at small obliqueness angles: In the intermediate range $10° < \theta < 65°$, the dependence on the angle is weak; at higher angles, a sharp drop occurs. In a study by Schneider (1989) heating

elements were used to force oblique waves into a boundary layer. The development of the oblique waves was then followed by measuring the shear stress. The saturation of the measured oblique waves versus the obliqueness angle was qualitatively the same as obtained here.

5.2. Presence of the Plane Wave

We will now examine the simultaneous development of the plane and oblique waves while the Reynolds number is frozen. The development of the waves at $\theta = 60°$ is described by equations (4.10) and (4.19), which are subject to the following initial conditions: amplitude of the oblique wave, $|A_i|$; amplitude of the plane wave, $|A_{oi}|$; and initial phase of the plane wave, ψ_{oi}. The initial phase angle of the oblique wave is taken to be zero. The initial detuning factor, k_i, is taken to be zero and $\psi_{oi} = 3\pi/2$.

Figure 7 shows the development of the oblique waves for the fully interactive case. The initial conditions are $\bar{R}/\bar{R}_{up} = 0.8$, $A_{oi} = 1$, and $A_i = 0.0001$. In figure 7(a), the oblique waves' amplitude is compared with the amplitude of the linear-growth case and with that of the parametric resonance case (only the linear and resonance terms are kept in (4.10)). The initial growth of the amplitude is identical to the linear one; however, the first stage of nonlinear interaction, caused by the parametric resonance mechanism (the second term in eq. (4.10)), soon comes into effect, causing exponential-of-exponential growth. As the amplitude increases, a second stage of interaction (the last term in eq. (4.10)) comes into effect wherein the self-interaction of the oblique waves reduces their growth rate and leads to their saturation.

In the linear-growth regime, the phase of the oblique waves' amplitude remains zero. In the resonance regime, if $\psi_{oi} = 3\pi/2$, the phase still remains zero, as depicted in figure 7(b). As the fully interactive stages occur, the phase decreases with $\bar{x}$, indicating a nonlinear influence on the streamwise wavenumber.

Figure 8 depicts the development of the plane wave under the same initial conditions as in figure 7. In the fully interactive stage, the amplitude of the plane wave is reduced compared to that of the linear growth (fig. 8(a)). However, the effect on the plane wave of the interactions is not as pronounced as in the case of the oblique waves. In the plane-wave equation (4.19), the coefficient of the A_0AA^* term is purely imaginary and, consequently, merely results in a nonlinear detuning of the streamwise wavenumber. Also, the back-reaction term is a quartic-type, A^4. Thus, the effect of nonlinearity on the plane wave is felt farther downstream, when the oblique waves reach a considerable amplitude. As for the phase of the plane-wave amplitude, figure 8(b) shows that it remains equal to its initial value up to the second stage of interaction, when it decreases in the downstream direction.

Figures 7 and 8 show that the development of the waves can be divided into distinct stages, according to the mechanisms involved. In the initial stage, the linear-growth mechanism governs. In the following, the parametric resonance mechanism governs. The plane wave still follows the linear theory but causes exponential-of-exponential growth of the oblique waves. As the oblique waves continue to grow, the fully interactive regime comes into effect. The

oblique waves react back on the fundamental, causing a reduction in its growth rate. The most important mechanism in the fully interactive regime is the oblique waves' self-interaction.

6. DISCUSSION AND CONCLUSIONS

The effects of critical-layer nonlinearity (CLN) on a near-resonance, spatially growing triad of instability waves comprised of a plane wave at fundamental frequency and a pair of symmetrical oblique waves at the subharmonic frequency were analyzed for a Blasius boundary layer. A low-frequency, high-Reynolds-number scaling in terms of the small parameter $\sigma \sim \bar{R}^{1/10}$ leads to a stability structure with a distinct critical layer, wherein nonlinearity is important.

In the fully interactive case, the amplitude of the oblique waves may exceed that of the plane wave such that a nonzero backreaction on the latter occurs. The amplitude equations were determined first by obtaining the analytical solutions for each term in the asymptotic expansion of the nonlinear viscous critical-layer flow. Then, to match the solutions, the velocity jump across the critical layer, calculated from the nonlinear (inner) solution within the critical layer, was equated to the velocity jump across the critical layer calculated from the linear (outer) solution. Eliminating the velocity jump yielded a direct, nonlinear relationship between the growth rates and the amplitudes.

The effort involved is justified by a comparatively simple amplitude equation that differs from previously obtained equations. For one, the resulting theory is fully nonlinear in that all the nonlinearly generated oscillatory and nonoscillatory components produced by the interactions are accounted for. The analysis indicated that when the amplitude of the oblique waves is smaller or comparable to that of the plane wave, a parametric resonance term appears in the amplitude equation for the subharmonic oblique waves. But the backreaction on the plane fundamental wave cancels out, even when the amplitudes are of the same order. A new stage of interaction comes into effect when the amplitude of the oblique waves becomes greater than that of the plane wave divided by $\sigma^{2.5}$; the growth rates become fully coupled with a nonzero backreaction term affecting the plane fundamental wave. This is also the same order of magnitude at which the oblique waves self-interaction comes into effect.

The development of the oblique waves in the absence of the plane wave was first examined in §5.1, where an analytical solution (5.3) was presented for the amplitude equation. This type of interaction in free shear flow was first considered by Goldstein & Choi (1989). The solution indicates that the saturation and decay of the oblique waves occur as a result of their self-interaction, a mechanism that does not require the presence of a plane wave or the appearance of a staggered pattern and that has not previously been identified in the subharmonic route to boundary-layer transition.

The study also indicated that, because the oblique waves initially follow the linear theory, their amplitude at first remains real, as originally prescribed. However, as the nonlinear effects become increasingly important downstream, the amplitude changes from real to complex, indicating a nonlinear modification of the streamwise wavenumber. Equilibrium occurs on the short nonlinear length scale when the linear-growth mechanism is balanced by the

self-interaction mechanism. The saturation level of the oblique waves is independent of their initial level but would slowly decrease on the long length scale on which the Reynolds number increases.

The saturation level of oblique waves was found to decrease with an increase in the obliqueness angle. As in the experimental data of Schneider (1989), increasing the obliqueness angle from zero to a small value resulted in an abrupt change in the nonlinear breakdown mechanism. The critical-layer singularity of the oblique mode was found to be stronger than that of the plane mode, which caused the nonlinearity and saturation of the oblique waves to occur at a much smaller amplitude compared to that of the strictly two-dimensional wave (of zero obliqueness angle). The saturation and decay mechanism of the oblique modes was therefore found to differ from that of the plane wave. This result is in agreement with that found by Goldstein & Choi (1989) for oblique waves in free shear flows where the nonlinear interaction leads to explosive growth.

Section 5.2 presented the results for the nonlinear mechanisms in the presence of the plane wave. The nonlinear effects were found to appear in two stages. In the first, the presence of the plane wave caused exponential-of-exponential growth of the oblique waves as a result of the parametric resonance mechanism. The oblique waves did not react back on the plane wave, allowing the latter to develop according to the linear theory, even when the oblique waves attained amplitudes on the same order of magnitude as the amplitude of the plane wave. However, as the oblique waves continued to grow and exceeded a certain level compared to that of the plane wave, a second fully interactive stage occurred. The growth rates became fully coupled and the oblique waves saturated because of their self-interaction while reacting back on the plane wave.

Part II of this study will present results for the composite solution, which accounts for both the flow-divergence and the nonlinear effects. Therein, excellent agreement with observations is demonstrated not only over the parametric resonance stage, but also over the fully interactive saturation and decay stages. Novel features of the phenomena will be discussed and new interpretations of the experimental data will be given.

APPENDIX A

LINEAR SOLUTION

We present here the details of the linear solution in the five-zoned structure.

A.1. Solution in Viscous Sublayer (Zone I)

For the viscous effects to come into play in this region, the scaling for y should be

$$y' = \sigma^4 \hat{y} \ , \tag{A.1.1}$$

where $\hat{y}$ is order one. This scaling is consistent with the classical theory result that the thickness of the wall layer is of the order $(\alpha RC)^{1/2}$ (Reid, 1965). Substituting equation (2.1) into the Orr-Sommerfeld equation, we obtain, up to the required order of approximation,

$$\left[\hat{D}^4 - i\hat{\alpha}\bar{R}(\lambda\sigma^3\hat{y} - \hat{c})\hat{D}^2\right]\hat{\Phi} = 0 \ , \tag{A.1.2}$$

where $\hat{\Phi}$ stands for Φ_0 or Φ, $\hat{\alpha}$ stands for $\bar{\alpha}$ or $\bar{\gamma}$, $\hat{c}$ stands for $\bar{c}_0$ or $\bar{c}$, and $\hat{D}$ is the derivative with respect to $\hat{y}$. We expand $\hat{\Phi}$ as

$$\hat{\Phi} = g_0 + \sigma g_1 + \sigma^2 g_2 + \sigma^3 g_3 + \ . \ . \ . \tag{A.1.3}$$

and, with $\hat{\alpha}$ and $\hat{c}$ expanded according to equation (2.7), we obtain

$$\left(\hat{D}^4 + i\bar{R}\tilde{\alpha}\tilde{c}_0\hat{D}^2\right)g_0 = 0 \ . \tag{A.1.4}$$

The solution of (A.1.4) must decay as $\hat{y} \to \infty$ and is subject to the conditions

$$g_0(0) = g_0'(0) = 0 \ . \tag{A.1.5}$$

The first-order solution is thus given by

$$g_0 = \frac{b_0}{m}\left(m\hat{y} - 1 + e^{-m\hat{y}}\right) \ , \tag{A.1.6}$$

$$m^2 = -i\bar{\alpha}\bar{R}\bar{c}_0 \ , \tag{A.1.7}$$

where b_0 is an arbitrary constant to be determined by matching with the solution at zone II. A similar solution is obtained for the oblique waves. The corresponding velocity components are given by

$$u = Re\left[\varepsilon A_0 b_0\left(1 - e^{-m\hat{y}}\right)e^{iX} + 2\delta Ab\cos\theta\cos Z\left(1 - e^{-M\hat{y}}\right)e^{iX/2} + \ldots\right] \tag{A.1.8}$$

$$v = Re\left[-i\sigma^5\bar{\alpha}\frac{b_0}{m}\left(m\hat{y} + e^{-m\hat{y}} - 1\right)\varepsilon A_0 e^{iX}\right.,$$

$$\left. - 2i\sigma^5\bar{\gamma}\frac{b}{M}\left(M\hat{y} + e^{-M\hat{y}} - 1\right)\delta A\cos Z\, e^{iX/2} + \ldots\right], \tag{A.1.9}$$

and

$$w = Re\left[2ib\sin Z\sin\theta\left(1 - Me^{-M\hat{y}}\right)\delta A e^{iX/2} + \ldots\right], \tag{A.1.10}$$

where

$$M^2 = -i\bar{\gamma}\bar{R}\bar{c}\ . \tag{A.1.11}$$

A.2. The Tollmien Region (zone II)

As pointed out by Goldstein, Durbin, & Leib (1987), the solution for this region is obtained by introducing the scaled transverse coordinate

$$Y = \frac{y}{\sigma} \tag{A.2.1}$$

directly into the Orr-Sommerfeld equation and using equations (2.1) and (2.7). The solution is obtained in the form

$$\hat{\Phi} = \sigma\left[\left(c_1 + \sigma c_2 + \sigma^2 c_3\right) + \left(c_2 + \sigma c_4 + \sigma^2 c_6\right)Y\right] + \sigma^4 F\ . \tag{A.2.2}$$

As will be shown, the matching requirements give $c_1 = c_2 = c_3 = 0$; therefore, the solution can be written as

$$\hat{\Phi} = \sigma(\lambda + \sigma a)Y + \sigma^4 F(Y,\phi)\ , \tag{A.2.3}$$

where a is an order-one constant that depends on σ, and F satisfies the relation

$$\frac{\partial^2 F}{\partial Y^2} = \mu_c\left(1 + \frac{Y_c}{Y - Y_c}\right) - \frac{1}{4}\lambda^2 Y(Y_c + Y)\ , \tag{A.2.4}$$

where

$$\mu_c = -\frac{\lambda^2 Y_c^2}{4} \tag{A.2.5}$$

and $\bar{c} = \lambda Y_c$.

Since equation (A.2.4) is singular at $Y = Y_c$, F can be discontinuous across Y_c, and $F^{\pm}$ denotes the solution above or under this point. Integrating equation (A.2.4), we obtain

$$F^{\pm}(Y,\phi) = F(0) + \mu_c \left\{ \frac{1}{2} Y^2 + Y_c \left[(Y - Y_c)\left(\ln|Y - Y_c| + i\hat{\phi}^{\pm} \right) + Y_c\left(\ln Y_c + i\hat{\phi}^{-} \right) \right] \right\} - \frac{\lambda^2}{4 \cdot 3!} Y^3 \left(Y_c + \frac{1}{2} Y \right), \tag{A.2.6}$$

where the normal velocity is continuous across the critical layer. The constants of integration $\phi^{\pm}$ and $\phi_0^{\pm}$ are, in general, a complex function of x_1. The value of F as $Y \to 0$ is $F(0)$, which is determined via matching with the solution in zone I. The corresponding velocity components are given by

$$u = Re\, \varepsilon A_0 \left[(\lambda + \sigma a) + \sigma^3 F(Y,\phi) \right] e^{iX} + 2\delta A \cos Z \left[(\lambda + \sigma a)\cos\theta + \frac{U'}{U - c} \times \sin\theta \tan\theta\, \sigma(\lambda + \sigma a)Y + \sigma^3 \cos\theta\, F'(Y,\phi) + \sigma^4 \frac{U'}{U - c} \sin\theta \tan\theta\, F(Y,\phi) \right] e^{iX/2}, \tag{A.2.7}$$

$$v = Re \left\{ -\varepsilon A_0 i\bar{\alpha}\sigma^2 \left[(\lambda + \sigma a_0)Y + \sigma^3 F(Y,\phi) \right] e^{iX} - 2\delta A i\bar{\gamma}\sigma^2 \left[(\lambda + \sigma a)Y + \sigma^3 F(Y,\phi) \right] \cos Z\, e^{iX/2} \right\}, \tag{A.2.8}$$

and

$$w = Re \left\{ 2i\, \delta A \sin Z \sin\theta \left[(\lambda + \sigma a) - \frac{U'}{U - c} \sigma(\lambda + \sigma a)Y + \sigma^3 F(Y,\phi) - \frac{U'}{U - c} \sigma^4 F(Y,\phi) \right] e^{iX/2} \right\}. \tag{A.2.9}$$

A.3. Solution in the Heisenberg Region (Zones IV and V)

According to Goldstein, Durbin, & Leib (1987), Miles' (1962) solution, which is uniformly valid for $y = O(1)$ and $y \gg 1$ in the limit as $\alpha,\gamma \to 0$, is given by

$$\frac{D\hat{\Phi}}{\hat{\Phi}} = \frac{U'}{U - \hat{c}} - \frac{1}{(U - \hat{c})^2\Omega^*} + O(\hat{\alpha}^5) \ , \tag{A.3.1}$$

where

$$\Omega^* = \frac{1}{\hat{\alpha}(1 - \hat{c})^2} + \Omega_o + \hat{\alpha}\Omega_1 + \hat{\alpha}^2\Omega_2 + \ldots \ , \tag{A.3.2}$$

$$\Omega_o = -\frac{1}{(1 - \hat{c})^2}\int_y^\infty \left[\frac{(U - \hat{c})^2}{(1 - \hat{c})^2} - \frac{(1 - \hat{c})^2}{(U - \hat{c})^2}\right]dy \ , \tag{A.3.3}$$

$$\Omega_1 = -\frac{2}{(1 - \hat{c})^2}\int_y^\infty (U - \hat{c})^2\Omega_o dy \ , \tag{A.3.4}$$

and

$$\Omega_2 = -\int_y^\infty (U - \hat{c})^2\left[\frac{2\Omega_1}{(1 - \hat{c})^2} + \Omega_o^2\right]dy \ . \tag{A.3.5}$$

By substituting equations (A.3.1) to (A.3.4) into the classical "inviscid function" Lin, 1955, p. 37), which is defined as

$$W \equiv \frac{\hat{c}D\hat{\Phi}}{U'\hat{\Phi} - (U - \hat{c})D\hat{\Phi}} \ , \tag{A.3.6}$$

and by inserting $U = U_B$ and equation (2.7) into the result, expanding for small σ, and then using equation (2.1), we obtain (following Goldstein, Durbin, & Leib, 1987)

$$W = W^\dagger(y;\sigma,\bar{c},\bar{\gamma}) + \sigma^3\,\frac{i\bar{c}\bar{\lambda}}{\bar{\gamma}^2}\left(\cos\theta + \frac{1}{\cos\theta}\right)\frac{A'}{A} \ , \tag{A.3.7}$$

and

$$W_o = W^\dagger(y;\sigma,\bar{c}_o,\bar{\alpha}) + \sigma^3\,\frac{2i\bar{c}\bar{\lambda}}{\bar{\alpha}^2}\frac{A_o'}{A_o} \ , \tag{A.3.8}$$

where

$$W^{\dagger}(y;\sigma,\bar{c},\hat{\alpha}) = \frac{U'\bar{c}}{\hat{\alpha}}(1-\sigma\bar{c})^{-2} - \frac{\sigma\bar{c}\lambda}{(1-\sigma\bar{c})^4}\left[J_1 + 2\sigma\bar{c}J_2 + \sigma^2\bar{c}^2J_3 + \frac{1}{8\lambda}y^2 + O(y^3)\right]$$

$$+ \sigma^2\hat{\alpha}\bar{c}\lambda\left[J_4 + \sigma\bar{c}J_5 - \frac{1}{4\lambda^3}y + O(y^2)\right] + \sigma^3\bar{c}\left[\frac{\bar{\mu}_c}{\lambda^2}\ln y - \frac{7}{48}\frac{\bar{c}^2}{\lambda^2} + O(y)\right] . \tag{A.3.9}$$

The coefficients J_1 to J_5 in the above equation are given by

$$J_1 \equiv \int_0^{\infty}\left[U_B^2 - \frac{1}{U_B^2} + \frac{1}{(\lambda y)^2}\right]dy , \tag{A.3.10a}$$

$$J_2 \equiv -\int_0^{\infty}\left[\frac{1}{U_B^3} - \frac{2}{U_B^2} + U_B - \frac{1}{(\lambda y)^3} + \frac{2}{(\lambda y)^2}\right]dy , \tag{A.3.10b}$$

$$J_3 \equiv \int_0^{\infty}\left[1 - \frac{2}{U_B^4} + \frac{8}{U_B^3} - \frac{6}{U_B^2} + \frac{3}{(\lambda y)^4} - \frac{8}{(\lambda y)^3} + \frac{6}{(\lambda y)^2} + \frac{1}{4\lambda^3 y(y+1)}\right]dy , \tag{A.3.10c}$$

$$J_4 \equiv 2\int_0^{\infty} U_B^2\int_0^{\infty}\left(U_B^2 - \frac{1}{U_B^2}\right)dy\,dy , \tag{A.3.10d}$$

$$J_5 \equiv \lim_{\substack{y\to 0\\ \hat{c}\to 0\\ U\to U_B}}\left(\frac{\partial\Omega_1}{\partial\hat{c}} + \lambda\Omega_2\right) . \tag{A.3.10e}$$

A.4. Matching Solutions

Matching the solution in zone I and the solution in zone II is easily done by matching the velocities. Considering the inner solution for the two-dimensional wave ((A.1.8) to (A.1.10)), as $\hat{y} \to \infty$, the solution reduces to

$$u = Re\ b_o e^{iX} , \tag{A.4.1}$$

$$v = Re\left[-i\alpha\sigma^5 b_o\left(\hat{y} - \frac{1}{m}\right) + \ldots\right]e^{iX} . \tag{A.4.2}$$

Considering the solution in zone II ((A.2.7) to (A.2.9)), as $Y \to 0$, we have

$$u = Re\left[\lambda + \sigma a + \sigma^3 F'(0) + \ldots\right]e^{iX} , \tag{A.4.3}$$

$$v = Re\left[-i\sigma^5 \bar{\alpha}_o F'(0) + \ldots\right]e^{iX} . \tag{A.4.4}$$

Matching the u-velocities gives

$$b_o = \lambda , \tag{A.4.5}$$

while matching the v-velocities gives the imaginary part of $F(0)$ as

$$F_i(0) = \frac{-\lambda}{\sqrt{2\bar{c}_o \bar{R}\bar{\alpha}}} . \tag{A.4.6}$$

Matching the velocities of the oblique waves produces similar expressions, with $\bar{c}$ replacing $\bar{c}_o$ and $\bar{\gamma}$ replacing $\bar{\alpha}$.

Matching the solution in zone II and the outer solution in zones IV and V is most easily done by using the inviscid function. The inviscid function for the solution in zone II is obtained by substituting equation (A.2.3) into equation (A.3.6) and re-expanding

$$\hat{W} = \frac{U}{\lambda} + \sigma^3\left[\frac{\mu_c Y_c}{\lambda}\left(\ln\frac{Y - Y_c}{Y_c} - i\Delta\hat{\phi}\right) - \frac{F(0)}{\lambda Y_c} - \frac{1}{8}\lambda Y_c Y(2Y_c + Y)\right] + O(\sigma^4) \tag{A.4.7}$$

for $Y > Y_c$, where $\Delta\hat{\phi}$ denotes either $\left(\phi^- - \phi^+\right)$ or $\left(\phi_o^- - \phi_o^+\right)$. Matching equations (A.3.7) and (A.3.8) shows that

$$\bar{\gamma} = \bar{\alpha} + \sigma^3 2\, Im\frac{A_o'}{A_o} + O(\sigma^4) \tag{A.4.8}$$

$$\lambda \frac{\bar{c}}{\bar{\alpha}}(1-\sigma\bar{c})^{-2} - 1 - \frac{\sigma\bar{c}\lambda}{(1-\sigma\bar{c})^4}\left(J_1 + 2\sigma\bar{c}J_2 + \sigma^2\bar{c}^2J_3\right) + \sigma^2\bar{\alpha}\bar{c}\lambda\left(J_4 + \sigma\bar{c}J_5\right)$$

$$+ \sigma^3\left[\bar{c}\left(\frac{\bar{\mu}_c}{\lambda}\ln Y_c - \frac{7}{48}\frac{\bar{c}^2}{\lambda^2} - \frac{2\lambda}{\bar{\alpha}^2}\mathcal{I}m\frac{A_o'}{A_o}\right) - \frac{F_r(0)}{\lambda Y_c} + \frac{Y_c^3}{4}\ln\sigma\right] = 0 \qquad (A.4.9)$$

$$\left(\cos\theta + \frac{1}{\cos\theta}\right)\frac{A'}{A} = -\frac{\bar{\gamma}^2\bar{\mu}_c}{\bar{c}\lambda^2}Y_c(\Delta\phi) + \frac{\bar{\gamma}^2}{\bar{c}\lambda Y_c\sqrt{2\bar{c}\bar{R}\bar{\gamma}}}\,, \qquad (A.4.10)$$

and

$$\frac{A_o'}{A_o} = -\frac{\bar{\alpha}^2\bar{\mu}_c}{2\bar{c}_o\lambda^2}Y_c(\Delta\phi_o) + \frac{\bar{\alpha}^2}{2\bar{c}_oY_c\lambda\sqrt{2\bar{c}_o\bar{R}\bar{\alpha}}} + i\,\mathcal{I}m\left(\frac{A_o'}{A_o}\right)_{initial}\,. \qquad (A.4.11)$$

Equations (A.4.8) and (A.4.9) are dispersion relations that determine $\bar{\alpha}$ and $\bar{\gamma}$ in terms of $\bar{c}$. Since their coefficients all are real, they are consistent with our original assertion that $\bar{\alpha}$ and $\bar{c}$ are real quantities. In fact, it follows from equations (2.5d) and (A.4.8) that

$$\bar{\beta} = \frac{\sqrt{3}}{2}\bar{\alpha} + \frac{4}{\sqrt{3}}\sigma^3\mathcal{I}m\frac{A_o'}{A_o} + O(\sigma^4)\,. \qquad (A.4.12)$$

This shows that $\bar{\beta}$ and $\bar{\alpha}$ satisfy the usual long-wavelength, small-growth-rate resonance condition to within the order of the detuning. To a first-approximation, equation (A.4.9) shows that $\bar{c}_o$ and $\bar{\alpha}$ satisfy the usual long-wavelength, small-growth-rate dispersion relation

$$\bar{c}_o = \frac{\bar{\alpha}}{\lambda}\,. \qquad (A.4.13)$$

The imaginary part of the dispersion relations (i.e., the matching between zones II and III) produces the real parts of equations (A.4.10) and (A.4.11). For the initial linear growth, $\Delta\hat{\phi}$ is real. The amplitude A is real, and A_o is initially complex, but its imaginary part remains equal to its initial value. Nonlinearity causes both amplitudes to become complex. Since the amplitudes appear as order σ^3 in the dispersion relations, the imaginary parts of A'/A or A_o/A_o are balanced by the imaginary part of the corresponding $\Delta\phi$. Therefore, equations (A.4.10) and (A.4.11) in their complex form are valid for both the linear and nonlinear growth regimes. They relate the slow growth rates of the instability waves A'/A and A_o/A_o to the phase jumps $\Delta\phi$ and $\Delta\phi_o$ across the critical layer. To determine these letter quantities, it is necessary to consider the flow in the critical layer.

Equations (A.2.3), (A.2.6) to (A.2.9), (A.4.5), and (A.4.6) show that the flow field in zone II can be written as

$$u = \sigma\lambda Y - \sigma^4 \frac{Y^2}{2}\left(\frac{\lambda^2}{4!} Y^2\right) + Re\left\{\left[\lambda + \sigma a_o + \sigma^3\left(f' + i\mu_c Y_c \phi_o^{\pm}\right)\right]\varepsilon A_o e^{iX} + 2\left(\frac{\lambda + \sigma a}{\cos\theta}\right.\right.$$

$$+ \frac{\bar{c}(\lambda + \sigma a)}{\lambda Y - \bar{c}} \tan\theta \sin\theta + \sigma^3\left\{f' \cos\theta + \frac{\tan\theta \sin\theta}{\lambda Y - \bar{c}}\left\{\lambda F(0) + \bar{\mu}_c \bar{c}\right.\right.$$

$$\times \left[(Y - Y_c)\ln|Y - Y_c| + Y_c \ln Y_c\right] + \lambda Y^2\left[\frac{1}{2}\mu_c - \frac{\lambda^2 Y}{4!}\left(Y_c + \frac{5}{2} Y\right.\right.$$

$$\left.\left.\left.\left.\left. - \frac{\lambda}{\lambda Y - \bar{c}} \frac{Y^2}{2}\right)\right]\right\} + \frac{\lambda A'}{\bar{\gamma} i A} \sin^2\theta\left[1 - \frac{\lambda Y}{\lambda Y - \bar{c}}\left(1 + \frac{\lambda Y}{\lambda Y - \bar{c}} \frac{1}{\cos^2\theta}\right)\right]\right.\right.$$

$$\left.\left.\left. + \frac{i\bar{\mu}_c Y_c}{\cos\theta}\left(\phi^{\pm} + \frac{\bar{c}}{\lambda Y - \bar{c}} \phi^{-} \sin^2\theta\right)\right)\right)(\cos Z)\delta A e^{iX/2}\right\} + \ldots \qquad \text{(A.4.14)}$$

$$v = -\sigma^2 \lambda Y \, Re\left[i\bar{\alpha}\varepsilon A_o e^{iX} + 2i\bar{\gamma}(\cos Z)\delta A e^{iX/2}\right] + \ldots \qquad \text{(A.4.15)}$$

$$w = -2\delta(\sin\theta \sin Z) \, Re \frac{\bar{c}\lambda}{\lambda Y - \bar{c}} i A e^{iX/2} + \ldots \qquad \text{(A.4.16)}$$

$$p = \sigma\bar{c}\lambda \, Re\left[\varepsilon A_o e^{iX} + 2(\cos\theta \cos Z)\delta A e^{iX/2}\right] + \ldots, \qquad \text{(A.4.17)}$$

where

$$f' = \mu_c\left(Y + Y_c \ln|Y - Y_c| + Y_c\right) - \frac{\lambda^2}{2} Y^2\left(\frac{Y_c}{4} + \frac{Y}{3!}\right). \qquad \text{(A.4.18)}$$

APPENDIX B

NONLINEAR SOLUTION AT THE s^8 LEVEL

At the σ^8 level, equation (3.11) gives

$$-\frac{1}{\bar{R}}\frac{\partial^2}{\partial\bar{\eta}^2}U_8^{(02)} = \frac{1}{2}\bar{c}\bar{\gamma}(A^*Q_{\bar{\eta}} + AQ_{\bar{\eta}}^*) \ , \tag{B.1}$$

$$\left(\bar{\alpha}\lambda\bar{\eta}i - \frac{1}{\bar{R}}\frac{\partial^2}{\partial\bar{\eta}^2}\right)U_8^{(20)} = 2\bar{\beta}i\tan\theta\, Q^2 - \bar{c}\bar{\gamma}A\tan\theta\, Q_{\bar{\eta}} \ , \tag{B.2}$$

$$\left(\bar{\alpha}\lambda\bar{\eta}i - \frac{1}{\bar{R}}\frac{\partial^2}{\partial\bar{\eta}^2}\right)U_8^{(22)} = -\frac{1}{2}\bar{c}\bar{\gamma}A\tan\theta\, Q_{\bar{\eta}} \ , \tag{B.3}$$

$$-\frac{1}{\bar{R}}\frac{\partial^2}{\partial\bar{\eta}^2}W_8^{(02)} = 2\bar{\beta}iQQ^* - \frac{1}{2}\bar{c}\bar{\gamma}(A^*Q_{\bar{\eta}} - AQ_{\bar{\eta}}^*) \ , \tag{B.4}$$

$$V_{8,\bar{\eta}}^{(02)} = -2i\bar{\beta}W_8^{(02)} \ , \tag{B.5}$$

$$V_{8,\bar{\eta}}^{(20)} = -\bar{\alpha}iU_8^{(20)} \ , \tag{B.6}$$

$$U_8^{(00)} = 2U_8^{(02)} \ , \tag{B.7}$$

$$U_8^{(2-2)} = U_8^{(22)} \ , \tag{B.8}$$

$$\sin\theta\, W_8^{(22)} = -\cos\theta\, U_8^{(22)} \ , \tag{B.9}$$

$$W_8^{(2-2)} = -W_8^{(22)} \ , \tag{B.10}$$

$$U_8^{(1\pm1)} = W_8^{(20)} = W_8^{(00)} = W_8^{(1\pm1)} = V_{8,\bar{\eta}}^{(00)} = V_{8,\bar{\eta}}^{(2\pm2)} = V_{8,\bar{\eta}}^{(1\pm1)} = 0 \ . \tag{B.11}$$

The substitution (eq. ((4.5)) and Fourier transform, defined as

$$\hat{F}(k) = \int_{-\infty}^{\infty} e^{-ik\eta}F(\eta)d\eta \ , \tag{B.12}$$

$$F(\eta) = \frac{1}{2\pi}\int_{-\infty}^{\infty} e^{ik\eta}\hat{F}(k)dk \ , \tag{B.13}$$

are used to obtain the solution for equations (C.1) to (C.6) as

$$U_8^{(02)} = -dAA^*(S_1 + S_2) + b_1 \ , \tag{B.14}$$

$$W_8^{(02)} = dAA^*\left(4 \sin^2 \theta \, S_3 + S_1 - S_2\right) + b_2 \ , \tag{B.15}$$

$$U_8^{(20)} = 2d \frac{\bar{\beta}}{\bar{\alpha}} hA^2\left(2 \sin^2 \theta \, S_4 + S_5\right) + b_3 \ , \tag{B.16}$$

$$U_8^{(22)} = d \frac{\bar{\beta}}{\bar{\alpha}} hA^2 \, S_5 + b_4 \ , \tag{B.17}$$

$$V_8^{(20)} = 2\bar{\beta} \, d\bar{c}A^2 h\left(2 \sin^2 \theta \, S_6 + S_7\right) + b_5 \ , \tag{B.18}$$

$$V_8^{(02)} = 2\bar{\beta}\bar{c} \, dAA^*\left(4 \sin^2 \theta \, S_8 + S_9 - S_{10}\right) + b_6 \ , \tag{B.19}$$

where

$$d = \frac{i\bar{\beta}}{\bar{\alpha}\lambda\bar{c}h} \ , \tag{B.20a}$$

and

$$h = \frac{1}{\frac{\bar{\alpha}}{2}\lambda\bar{c}^3\bar{R}} \ , \tag{B.20b}$$

$$S_1 = \int_{-\infty}^{0} \frac{e^{ik\eta}}{k} e^{hk^3/3} \, dk \ , \tag{B.20c}$$

$$S_2 = -\int_{-\infty}^{0} \frac{e^{-ik\eta}}{k} e^{hk^3/3} \, dk \ , \tag{B.20d}$$

$$S_3 = \int\int_{-\infty}^{0} \frac{e^{\left[(h/3)\left(k_1^3+k_2^3\right)+i\left(k_1-k_2\right)\eta\right]}}{\left(k_1 - k_2\right)^2} \, dk_1 \, dk_2 \ , \tag{B.20e}$$

$$S_4 = \int\int\int_{-\infty}^{0} e^{\left[ik\eta+(h/6)k^3-(h/6)\left(k_1+k_2\right)^3+(h/3)\left(k_1^3+k_2^3\right)\right.} H\left(k_1 + k_2 - k\right)dk_1\, dk_2\, dk \ ,$$

(B.20f)

$$S_5 = \int\int_{-\infty}^{0} e^{\left[ik\eta+(h/6)\left(k_1^3+k^3\right)\right]} k_1 H\left(k_1 - k\right)dk_1\, dk \ , \qquad \text{(B.20g)}$$

$$S_6 = \int\int\int_{-\infty}^{0} \frac{1}{k}\, e^{\left[ik\eta+(h/6)k^3+(h/3)\left(k_1^3+k_2^3\right)-(h/6)\left(k_1+k_2\right)^3\right]}$$

$$\times H\left(k_1 + k_2 - k\right)dk_1\, dk_2\, dk \ , \qquad \text{(B.20h)}$$

$$S_7 = \int\int_{-\infty}^{0} \frac{k_1 e^{\left[ik\eta+(h/6)\left(k^3+k_1^3\right)\right]}}{k} H\left(k_1 - k\right)dk_1\, dk \ , \qquad \text{(B.20i)}$$

$$S_8 = \int\int_{-\infty}^{0} \frac{e^{\left[(h/3)\left(k_1^3+k_2^3\right)+i\left(k_1-k_2\right)\eta\right]}}{\left(k_1 - k_2\right)^3}\, dk_1\, dk_2 \ , \qquad \text{(B.20j)}$$

$$S_9 = \int_{-\infty}^{0} \frac{e^{ik\eta}}{k^2}\, e^{hk^3/3}\, dk \ , \qquad \text{(B.20k)}$$

$$S_{10} = -\int_{-\infty}^{0} \frac{e^{-ik\eta}}{k^2}\, e^{hk^3/3}\, dk \ , \qquad \text{(B.20ℓ)}$$

where H is the step function, and b_1 to b_6 are constants, determined through matching to the corresponding linear solution outside the critical layer.

APPENDIX C

VELOCITY JUMP FOR THREE-DIMENSIONAL MODE

Upon using equation (4.2) in equation (4.3), we obtain

$$2\left(i\frac{\bar{\alpha}}{2}\lambda\bar{\eta} - \frac{1}{\bar{R}}\frac{\partial^2}{\partial\bar{\eta}^2}\right)Q_{10.5}^{(11)} = \bar{c}A\gamma i\left[2\mu_c\cos\theta + \cos\theta\left(U_{8,\bar{\eta}\eta}^{(00)} + U_{8,\bar{\eta}\eta}^{(02)}\right) - \sin\theta\, W_{8,\bar{\eta}\eta}^{(02)}\right]$$

$$- \bar{c}A^*\gamma i\left(U_{8,\bar{\eta}\eta}^{(20)} + U_{8,\bar{\eta}\eta}^{+(22)}\right) + 2\bar{c}\bar{\alpha}\sin\theta\, A_o\, Q_{\bar{\eta}\eta}^{\pm}$$

$$+ 2\bar{\beta}\left[2\left(QU_8^{(02)}\right)_{\bar{\eta}}\cos\theta - \sin\theta\, Q_\eta W_8^{(02)}\right.$$

$$\left. + Q_\eta^*\left(U_8^{+(22)} + U_8^{(20)}\cos\theta\right)\right]$$

$$- 2\sin\theta\, i\left(Q_{\bar{\eta}\eta}\, V_8^{02} - Q_{\bar{\eta}\eta}^{\pm} V_8^{20}\right) . \qquad (C.1)$$

The solution Q at the 5.5 level is given by (4.4), whereas that at the σ^8 level is given in appendix B. Taking the Fourier transform of equation (C.1) gives

$$\hat{Q}_{10.5}^{(11)} = e^{hk^3/3}\int_k^\infty e^{-hk_1^3/3}\left(\hat{\zeta}_0 + \hat{\zeta}_1 + \hat{\zeta}_2 + \zeta_3\right)dk_1 , \qquad (C.2)$$

where

$$\zeta_0 = 2iA\frac{\bar{\gamma}}{\bar{\alpha}}\frac{\mu_c}{\bar{\lambda}}\cos\theta + \frac{2\sin\theta}{\lambda\bar{c}^2}A_oQ_{\eta\eta}^* , \qquad (C.3a)$$

$$\zeta_1 = i\frac{\bar{\gamma}}{\bar{\alpha}\,\lambda\bar{c}^2}\left(3A\cos\theta\, U_{8,\eta\eta}^{(02)} + A\sin\theta\, W_{8,\eta\eta}^{(02)} - A^*U_{8,\eta\eta}^{(20)}\cos\theta\right) , \qquad (C.3b)$$

$$\zeta_2 = \frac{2\bar{\beta}}{\bar{\alpha}\lambda\bar{c}^2}\left[2\left(QU_8^{(02)}\right)_\eta\cos\theta - Q_\eta W_8^{(02)}\sin\theta + Q_\eta^*U_{8,\eta}^{(20)}\cos\theta\right] , \qquad (C.3c)$$

$$\zeta_3 = \frac{2i\sin\theta}{\bar{\alpha}\lambda\bar{c}^3}\left(Q_{\eta\eta}^*V_8^{20} - Q_{\eta\eta}V_8^{02}\right) . \qquad (C.3d)$$

The velocity jump J_{3D} is obtained by

$$J_{3D} = \int_{-\infty}^{\infty} Q_{10.5}^{(11)}\, d\eta = \hat{Q}_{10.5}^{(11)}(k = 0) = J_0 + J_1 + J_2 + J_3 \,, \tag{C.4}$$

where

$$J_j = \int_0^{\infty} e^{-hk_1^3/3}\, \zeta_j\, dk_1, \quad j = 0, 1, 2, 3 \tag{C.5}$$

and

$$J_0 = 2\pi i A \frac{\bar{\gamma}}{\bar{\alpha}} \frac{\mu_c}{\lambda} \cos\theta + 2 \frac{\sin\theta}{\lambda \bar{c}^2} A_o I_o \tag{C.6a}$$

$$J_1 = \frac{\bar{\gamma}}{2\bar{\alpha}\lambda^2 \bar{c}^3 h} \left[-3(A^* I_1 + A I_2)A + \frac{2\bar{\beta}}{\bar{\alpha}} (A^* I_1 - A I_2)A + 8 \frac{\bar{\beta}^2}{\bar{\alpha}\bar{\gamma}} I_3 - 4 \frac{\bar{\beta}^2 h}{\bar{\alpha}\bar{\gamma}} A^* I_4 \right.$$

$$\left. - \frac{2h\bar{\beta}}{\bar{\alpha}} A^* A I_5 \right] \,, \tag{C.6b}$$

$$J_2 = \frac{1}{\pi\lambda^2} \frac{\bar{\beta}^3}{\bar{c}^3 h} \frac{}{\bar{\alpha}^2 \bar{\gamma}} \left(- \frac{\bar{\alpha}}{\bar{\beta}} \frac{\bar{\gamma}}{\bar{\beta}} I_6 - 4i I_7 - \frac{\bar{\gamma}}{\bar{\beta}} I_8 + 2ih I_9 + iAh \frac{\bar{\gamma}}{\bar{\beta}} I_{10} \right) \,, \tag{C.6c}$$

$$J_3 = \frac{2 \sin^2\theta}{\lambda^2 \bar{c}^3} \frac{\bar{\beta}^2}{\bar{\alpha}^2} \left[4A^* I_{11} + iAA^* \frac{\bar{\gamma}}{\bar{\beta}} I_{12} - \frac{8}{h} A I_{13} - \frac{2\bar{\gamma}}{\bar{\beta}} \frac{A}{h} I_{14} \right] \,, \tag{C.6d}$$

$$I_o = \int_0^{\infty} e^{-hk^3/3} \hat{Q}_{\eta\eta}^*\, dk \,, \tag{C.7a}$$

$$I_1 = -\int_{-\infty}^{0} e^{hk_1^3/3} k_1 \left[\hat{Q}(-k_1) \right] dk_1 \,, \tag{C.7b}$$

$$I_2 = -\int_{-\infty}^{0} e^{hk_1^3/3} k_1 \left[\hat{Q}^*(-k_1) \right] dk_1 \,, \tag{C.7c}$$

$$I_3 = \int_{-\infty}^{0} e^{hk_1^3/3} \left[\hat{Q}Q^*(-k_1)\right] dk_1 \ , \qquad \text{(C.7d)}$$

$$I_4 = \int_{-\infty}^{0} e^{hk_1^3/6} k_1^2 \int_{-k_1}^{\infty} e^{-hk_2^3/6} \hat{Q}^2 \, dk_2 \, dk_1 \ , \qquad \text{(C.7e)}$$

$$I_5 = \int_{-\infty}^{0} e^{hk_1^3/6} k_1^2 \int_{-k_1}^{\infty} e^{-hk_2^3/6} k_2 \hat{Q} \, dk_2 \, dk_1 \ , \qquad \text{(C.7f)}$$

$$I_6 = -\int_{-\infty}^{0} e^{hk_1^3/3} k_1 \int_{-\infty}^{\infty} e^{ik_1\eta} Q \int_{-\infty}^{\infty} \frac{1}{k_2} (A^*\hat{Q} + A\hat{Q}^*) e^{ik_2\eta} \, dk_2 \, dk \, d\eta \ , \qquad \text{(C.7g)}$$

$$I_7 = \int_{-\infty}^{0} e^{hk_1^3/3} \int_{-\infty}^{\infty} e^{ik_1\eta} Q_\eta \int_{-\infty}^{\infty} \frac{(\hat{Q}Q^*)}{k_2^2} e^{ik_2\eta} \, dk_2 \, dk_1 \, d\eta \ , \qquad \text{(C.7h)}$$

$$I_8 = \int_{-\infty}^{0} e^{hk_1^3/3} \int_{-\infty}^{\infty} e^{ik_1\eta} Q_\eta \int_{-\infty}^{\infty} \frac{(A^*\hat{Q} - A\hat{Q}^*)}{k_2} e^{ik_2\eta} \, dk_2 \, dk_1 \, d\eta \ , \qquad \text{(C.7i)}$$

$$I_9 = \int_{-\infty}^{0} e^{hk_1^3/3} \int_{-\infty}^{\infty} e^{ik_1\eta} Q_\eta^* \int_{-\infty}^{\infty} e^{\left(hk_2^3/6\right)+ik_2\eta} \int_{k_2}^{\infty} e^{-hk_3^3/6} \hat{Q}^2 \, dk_3 \, dk_2 \, dk_1 \, d\eta \ ,$$

$$\text{(C.7j)}$$

$$I_{10} = \int_{-\infty}^{0} e^{-hk_1^3/3} \int_{-\infty}^{\infty} e^{ik_1\eta} Q_\eta + \int_{-\infty}^{\infty} e^{\left(hk_2^3/6\right)+ik_2\eta} \int_{k_2}^{\infty} e^{-hk_3^3/6} k_3 \hat{Q}$$

$$\times \, dk_3 \, dk_2 \, dk_1 \, d\eta \ , \qquad \text{(C.7k)}$$

$$I_{11} = \iint_{-\infty}^{0} e^{\left(k_1^3+k_2^3\right)h/3} k_1^2 \int_{-\infty}^{\infty} \frac{e^{hk_3^3/2}}{k_3} \delta(k_3 - k_1 + k_2) \int_{k_3}^{\infty} e^{-hk_4^3/6} \tilde{Q}^2 \times dk_4\, dk_3\, dk_2\, dk_1 , \qquad (C.7\ell)$$

$$I_{12} = \iint_{-\infty}^{0} e^{\left(k_1^3+k_2^3\right)h/3} k_1^2 \int_{-\infty}^{\infty} \frac{e^{hk_3^3/2}}{k_3} \delta(k_3 - k_1 + k_2) \int_{k_3}^{\infty} e^{-hk_4^3/6} k_4 \hat{Q} \times dk_4\, dk_3\, dk_2\, dk_1 , \qquad (C.7m)$$

$$I_{13} = \iint_{-\infty}^{0} \int_{-\infty}^{\infty} \frac{k_1^2}{k_2^3} e^{(h/3)\left(k_1^3+k_3^3\right)} \hat{Q}\hat{Q}^* \delta(k_2 + k_1 + k_3) dk_2\, dk_1\, dk_3 , \qquad (C.7n)$$

$$I_{14} = \iint_{-\infty}^{0} \int_{-\infty}^{\infty} \frac{k_1^2}{k_2^2} \delta(k_2 + k_1 + k_3)[A^*\hat{Q} - A\hat{Q}^*] dk_2\, dk_1\, dk_3 , \qquad (C.7o)$$

where I_0 to I_{14} are given by equation (C.7). Substituting I_0 to I_{14} into equation (C.6), we obtain

$$J_0 = 2\pi i A \frac{\bar{\gamma}}{\bar{\alpha}} \frac{\mu_c}{\lambda} \cos\theta - 4\pi \sin^2\theta \frac{A_o A^*}{\lambda \bar{c}^2 h} T_o , \qquad (C.8a)$$

$$J_1 = \pi \frac{\bar{\beta}}{\bar{\alpha}} \frac{A^2 A^*}{\lambda^2 \bar{c}^3 h^{5/3}} \left[-\left(3 + \frac{2\bar{\beta}}{\bar{\alpha}}\right) T_2 + \frac{8\bar{\beta}^3}{\bar{\alpha}\bar{\gamma}^2} T_3 \right] , \qquad (C.8b)$$

$$J_2 = \frac{4\pi A^2 A^*}{\lambda^2 \bar{c}^3 h^{5/3}} \frac{\bar{\beta}^6}{\bar{\alpha}^2 \bar{\gamma}^4} \left[-\pi i T_7 - 2T_9 + \frac{\bar{\gamma}^2}{\bar{\beta}^2} T_{10} \right] , \qquad (C.8c)$$

$$J_3 = -\frac{8\pi A^2 A^*}{\lambda^2 \bar{c}^3 h^{5/3}} \frac{\bar{\beta}^6}{\bar{\alpha}^2 \bar{\gamma}^2} \left[-2T_{11} - 4T_{13} \right] . \qquad (C.8d)$$

The T's are the reduced form of the I integrals and are evaluated to give

$$T_0 = 0.5,\ T_2 = 0.591,\ T_3 = 0.73,\ T_7 = 1.03,\ T_9 = 0.0625,\ T_{10} = 0.188,$$

$$T_{11} = -\frac{\pi i}{32},\ T_{13} = -\frac{\pi i}{4} T_7 \ . \qquad \text{(C.9)}$$

Using $\bar{\alpha} = \sqrt{\lambda \bar{R}}$, $\bar{c} = \sqrt{\bar{R}/\lambda}$, and $\cos\theta = 1/2$, and substituting the numerical values for the integrals (C.9) in (C.8) we obtain

$$J_0 = -\frac{i\pi A}{4}\frac{\bar{R}}{\lambda^2} - \frac{3}{4}\pi \bar{R}^2 A_o A^* \ , \qquad \text{(C.10a)}$$

$$J_1 = 0.845\ \frac{A^2 A^* \bar{R}^{3.5}}{\sqrt{\lambda}} \ , \qquad \text{(C.10b)}$$

$$J_2 = (0.21 - 5.39i)\ \frac{A^2 A^* \bar{R}^{3.5}}{\sqrt{\lambda}} \ , \qquad \text{(C.10c)}$$

$$J_3 = -11.45i\ A^2 A^*\ \frac{\bar{R}^{3.5}}{\sqrt{\lambda}} \ . \qquad \text{(C.10d)}$$

Thus, we can write

$$J_1 + J_2 + J_3 = M\ \frac{A^2 A^* \bar{R}^{3.5}}{\sqrt{\lambda}} \ , \qquad \text{(C.11a)}$$

where

$$M = 1.055 - 16.8i \ . \qquad \text{(C.11b)}$$

The jump for the three-dimensional mode is thus given by

$$J_{3D} = -i\pi\ \frac{\bar{R}}{4\lambda^2} A - \frac{3}{4}\pi \bar{R}^2\ A_o A^* + M\ \frac{\bar{R}^{3.5}}{\sqrt{\lambda}} A^2 A^* \ . \qquad \text{(C.12)}$$

APPENDIX D

VELOCITY JUMP FOR THE TWO-DIMENSIONAL MODE

Substituting equation (4.14) into equation (4.13) and using the transformation (eq. ((4.5), we obtain

$$\left(2\eta i - h\frac{\partial^2}{\partial\eta^2}\right)Q_{13}^{(20)} = \frac{1}{\bar{\alpha}\bar{c}\lambda}\left(T_{M-8} + T_{8-8} + T_{5.5-10.5}\right) , \tag{D.1}$$

where T_{M-8} is the interaction of the mean flow with the σ^8-level components, given by

$$T_{M-8} = 2i\mu_c\bar{\alpha}\cos\theta\,\bar{c}A_o - \bar{\alpha}i\mu_c\bar{c}\eta^2 U_{8,\eta}^{(20)}\cos\theta - 2\mu_c\cos\theta\,V_8^{(20)} . \tag{D.2a}$$

The interaction among the 8-8 components is T_{8-8}

$$T_{8-8} = \frac{2i\bar{\alpha}}{\bar{c}}\Big(2\sin\theta\,W_8^{(02)}U_{8,\eta}^{(2-2)} - 2\cos\theta\,U_8^{(2-2)}U_{8,\eta}^{(02)} - \cos\theta\,U_8^{(02)}U_{8,\eta}^{(2-2)}$$

$$- \frac{1}{2}\cos\theta\,U_8^{(00)}U_{8,\eta}^{(20)}\Big) + U_{8,\eta\eta}^{(00)}\frac{\cos\theta}{\bar{c}^2}\left(\bar{c}A_o\alpha i - V_8^{20}\right)$$

$$- 2\cos\theta\,\frac{U_{8,\eta\eta}^{(2-2)}V^{(02)}}{\bar{c}^2} . \tag{D.2b}$$

$T_{5.5-10.5}$ is the interaction of the 5.5-level components with the 10.5-level components

$$T_{5.5-10.5} = \left[\frac{2i}{\bar{c}}A\bar{\gamma}\cos\theta\,U_{10.5,\eta\eta}^{(11)}\right] + \left[4\frac{\bar{\beta}}{\bar{c}}Q_\eta\left(U_{10.5}^{(11)}\cos\theta - W_{10.5}^{(11)}\sin\theta\right)\right]$$

$$+ \left[\frac{2\bar{\beta}}{\bar{c}}Q\left(3\cos\theta\,U_{10.5,\eta}^{(11)} - \sin\theta\,W_{10.5,\eta}^{(11)}\right)\right] - \left[\frac{2i}{\bar{c}^2}\sin\theta\,Q_{\eta\eta}V_{10.5}^{(11)}\right] . \tag{D.2c}$$

Other terms appearing in equation (4.13) do not contribute to the (20) component.

The equations for the U_8, W_8, and V_8 components are given in appendix B. The solution at the 10.5 level is obtained by utilizing equations (3.11) and (4.5) to obtain

$$\left(\eta i - h \frac{\partial^2}{\partial \eta^2}\right) U_{10.5}^{(11)} = \frac{R_u}{\bar{\alpha}\lambda\bar{c}} \tag{D.3a}$$

and

$$\left(\eta i - h \frac{\partial^2}{\partial \eta^2}\right) W_{10.5}^{(11)} = \frac{R_w}{\bar{\alpha}\lambda\bar{c}} \ , \tag{D.3b}$$

$$V_{\eta 10.5}^{11} = -i\bar{\gamma}\bar{c} U_{10.5}^{+(11)} \ , \tag{D.3c}$$

where

$$R_u = -\bar{\beta} f_1 + 5\bar{\beta} f_2 - \bar{\beta} \tan\theta \, f_3 + \bar{\alpha} A_o \tan\theta \, f_4 + i\bar{\gamma}(3A f_5 - A^* f_6)$$

$$- \frac{i}{\bar{c}} \tan\theta (f_7 - f_8) + 2i\mu_c \bar{\gamma} A \bar{c}^2 f_{10} + \frac{1}{2} \bar{\alpha} \tan\theta \, \mu_c \bar{c}^2 f_{11} \ , \tag{D.4a}$$

$$R_w = \frac{\bar{\alpha}}{2} f_1 - \frac{\bar{\alpha}}{2} f_2 + \bar{\beta} f_3 + \bar{\alpha} A_o f_4 - \frac{i}{\bar{c}} (f_7 - f_8) - \frac{\bar{\alpha}}{2} \mu_c \bar{c}^2 f_{11}$$

$$+ i\bar{\gamma}\left(A f_9 + \cos\theta \frac{A^* f_{12}}{\sin\theta}\right) \ , \tag{D.4b}$$

and

$$f_1 = Q^* U_8^{(20)} \ , \tag{D.4c}$$

$$f_2 = Q U_8^{(02)} \ , \tag{D.4d}$$

$$f_3 = Q W_8^{(02)} \ , \tag{D.4e}$$

$$f_4 = Q_\eta^* \ , \tag{D.4f}$$

$$f_5 = U_{8,\eta}^{(02)} \ , \tag{D.4g}$$

$$f_6 = U_{8,\eta}^{(20)} + U_{8,\eta}^{(22)} \ , \tag{D.4h}$$

$$f_7 = Q_{8,\eta} V^{(02)} \ , \tag{D.4i}$$

$$f_8 = Q_\eta^* V^{(20)} \ , \tag{D.4j}$$

$$f_9 = W_{8,\eta}^{(02)} \ , \tag{D.4k}$$

$$f_{10} = \eta \ , \tag{D.4ℓ}$$

$$f_{11} = Q\eta^2 \ , \tag{D.4m}$$

$$f_{12} = U_{8,\eta}^{(22)} \ . \tag{D.4n}$$

The Fourier transform of equation (E.1) is given by

$$\hat{Q}_{13}^{(20)} = \frac{e^{hk^3/6}}{2\bar{\alpha}\lambda\bar{c}} \int_k^\infty e^{-hk_1^3/6} \hat{R}_Q \, dk \ . \tag{D.5}$$

The velocity jump is given by

$$J_{2D} = \frac{1}{2\bar{\alpha}\lambda\bar{c}} \int_0^\infty e^{-hk_1^3/6} \hat{R}_Q \, dk \ , \tag{D.6a}$$

where

$$R_Q = T_{M-8} + T_{8-8} + T_{5.5-10.5} \ . \tag{D.6b}$$

The jump J_{2D} can be written as

$$J_{2D} = J_{M-8} + J_{8-8} + J_{5.5-10.5} \ , \tag{D.7}$$

where

$$J_{M-8} = \frac{\pi}{2} i \frac{\bar{\alpha}}{\bar{\gamma}} \frac{\mu_c}{\lambda} A_o = - \frac{\pi i}{4} \frac{\bar{R}}{\lambda^2} A_o \cos\theta \ . \tag{D.8}$$

This jump results from the mean-flow interaction with the linear part of $V_8^{(20)}$ component. The other terms in T_{M-8} (eq. (5.5)) produce no velocity jump. The J_{8-8} is given by

$$J_{8-8} = \frac{\pi}{2}\cos\theta\,\frac{\bar{\beta}}{\bar{\alpha}}\frac{1}{\sqrt{\lambda}}\left[A_0AA^*\bar{R}^{4.5}2^{1/3}I_{81} - \frac{2^{2/3}}{\sqrt{\lambda}}A^3A^*\frac{\bar{\beta}^2}{\bar{\alpha}^2}\bar{R}^5I_{82}\right], \qquad (D.9a)$$

where

$$I_{81} = \int_0^\infty x\,dx\,e^{-x^3/3}, \qquad (D.9b)$$

$$I_{82} = \iiint_0^\infty e^{-\frac{1}{6}\left[x^3+x_1^3+x_2^3\right]-\frac{1}{3}\left(x_1+x_2\right)^3}x_1H(x_2-x_1)dx_1\,dx_2\,dx, \qquad (D.9c)$$

and, substituting $\cos\theta = 1/2$, we obtain

$$J_{8-8} = 0.8567A_0AA^*\frac{\bar{R}^{3.5}}{\sqrt{\lambda}}I_{81} - 0.808\frac{A^*A^3}{\lambda}\bar{R}^5I_{82}. \qquad (D.9d)$$

The first term in the above equation results from the term in T_{8-8} involving $U_8^{(00)}$ alone interacting with the linear part of V_8^{20}. The second term in the above equation is the result of the term in T_{8-8} involving $U_8^{(2-2)}U_{8\eta}^{02}$. Other terms in T_{8-8} do not contribute to the velocity jump.

The jump resulting from the 5.5-10.5 interactions is written as

$$J_{5.5-10.5} = G_a + G_b + G_c. \qquad (D.10)$$

Jump G_a corresponds to the first square-bracketed term in equation (D.2c), jump G_b corresonds to the second square-bracketed term in equation (D.2c), and jump G_c corresponds to the third square-bracketed term in equation (5.7). The fourth square-bracketed term in equation (D.2c) produces no velocity jump. G is given by

$$G_a = -\pi\frac{\bar{\beta}}{\bar{\alpha}}\frac{A^3A^*}{\bar{\lambda}^3\bar{c}^4}\frac{1}{h^{7/3}}\left(\frac{2}{3}\frac{\bar{\beta}^2}{\bar{\alpha}^2}\sin\theta\,T_{a1} - 3\frac{\bar{\gamma}}{\bar{\alpha}}T_{a5}\right) + 2\pi\frac{\bar{\beta}^2}{\bar{\alpha}\bar{\gamma}}\frac{A_oA^*A}{\lambda^2c^3h^{5/3}}T_{a4} \qquad (D.11a)$$

$$G_b = 6\pi\left(\frac{\bar{\beta}}{\bar{\alpha}}\right)^2\frac{\sin\theta}{\bar{\lambda}^3\bar{c}^4}\frac{A^*A^3}{h^{7/3}}\left[2\frac{\bar{\beta}^2}{\bar{\alpha}^2}\sin\theta\,T_{b1} + \frac{\bar{\gamma}}{\bar{\alpha}}(3\cos\theta - \sin\theta)T_{b5}\right] \qquad (D.11b)$$

$$G_c = -\frac{4\pi\bar{\beta}^2}{\bar{\alpha}^2}\frac{A^*A^3}{\lambda^3\bar{c}^4h^{7/3}}\left[\frac{2\bar{\beta}^2}{\bar{\alpha}^2}\sin^2\theta\, T_{c1} + \frac{\bar{\gamma}}{2\bar{\alpha}}\sin\theta(6\cos\theta - \sin\theta)T_{5c}\right]$$

$$- \frac{4\pi\bar{\beta}}{\bar{\alpha}}\frac{A_oAA^*\sin^3\theta}{\lambda^2\bar{c}^3h^{5/3}}T_{4c} \,. \qquad \text{(D.11c)}$$

In the above equations, terms involving T_1 result from interaction with the $Q^*U^{(20)}$ constituent of the $U^{(11)}_{10.5}$ or $W^{(11)}_{10.5}$. Terms involving T_4 result from the interaction with the Q^*_η constituent of the 10.5 components, and terms involving T_5 result from the interaction with the $U^{(02)}_8$ or $W^{(02)}_8$ constituent of the 10.5 components. The jump resulting from the 5.5- to 10.5-level interactions is written as

$$J_{5.5\text{-}10.5} = N_1\frac{\bar{R}^{3.5}}{\sqrt{\lambda}}A_oA^*A + N_2\frac{\bar{R}^5A^*A^3}{\lambda}\,, \qquad \text{(D.12)}$$

where

$$N_1 = 1.48\,T_{a4} - 2.228\,T_{c4} = -0.2188 \qquad \text{(D.13a)}$$

and

$$N_2 = -0.2338\,T_{a1} + 1.62\,T_{a5} + 2.1\,T_{b1} + 1.026\,T_{b5} - 2.098\,T_{c1}$$

$$- 2.93\,T_{c5} = -0.15\,. \qquad \text{(D.13b)}$$

The total jump for the two-dimensional wave is given by

$$J = -\frac{\pi i}{8}\frac{\bar{R}}{\lambda^2}A_o + M_1\bar{R}^{3.5}\frac{A_oA^*A}{\sqrt{\lambda}} + M_2\frac{\bar{R}^5}{\lambda}A^*A^3\,, \qquad \text{(D.14)}$$

where

$$M_1 = 0.5848 \qquad \text{(D.15a)}$$

$$M_2 = -0.241\,. \qquad \text{(D.15b)}$$

APPENDIX E

INTERACTION MECHANISMS CONTRIBUTING TO AMPLITUDE EQUATIONS

Equations (4.10) and (4.19) represent the development of the oblique and plane waves, respectively. The interaction mechanisms leading to these equations will be discussed here.

E.1. Oblique Waves

Equation (4.10) indicates that there are three mechanisms governing the development of oblique waves. Its first term represents the usual linear growth; its second term represents the fundamental-subharmonic interaction that results from the interaction of the v_8^{20} component of the plane waves with the 5.5 components of the oblique waves; its last term represents the oblique waves' self-interaction.

The oblique waves' self-interaction term results from the velocity jumps across the critical layer, J_1, J_2, and J_3, given in appendix C: J_1 results from the interaction of the $V_{5.5}^{(1\pm1)}$ component with $U_8^{(02)}$ and $W_8^{(02)}$; J_2 results from the interaction of the $(5.5)^{(1-1)}$ components with $W_8^{(02)}$ and from the interaction of the $(5.5)^{(-11)}$ components with $U_8^{(20)}$; and J_3 results from the interaction of the V_8 terms produced by nonlinearity with $U_{5.5}$, that is, from the interaction of $V_8^{(02)}$ with $(5.5)^{(1-1)}$ components and from the interactions of $V_8^{(20)}$ with the $(5.5)^{(-11)}$ terms. (These interactions are summarized in table I.)

F.2. Plane Wave

The plane wave's nonlinear development is governed by the jump across the critical layer. For the sake of discussion, this jump was split into three separate mechanisms: J_{M-8}, J_{8-8}, and $J_{5.5-10.5}$. (These interactions are depicted in table II.)

J_{M-8} (eq. (D.8) represents the usual linear growth. This jump results from the linear part of the V_8^{20} component interacting with the mean flow. The other 8 components interacting with the mean flow produce no jump.

The second type of interaction, J_{8-8} (eq. (D.9), results from the self-interaction of the 8 components. The 5.5 components first self-interact to produce several 8 components: $U_8^{(nm)}$, $V_8^{(nm)}$, and $W_8^{(nm)}$, with nm = (02), (20), (22), (00), (2±2), and (1±1). The U_8^{00} component interacts with the linear part of the V_8^{20} component to produce the first term in J_{8-8} (eq. (5.30)). The U_8^{2-2} interacts with the $U_8^{(02)}$ to produce the second term in J_{8-8}. Other 8 components produce no velocity jump.

The third nonlinear mechanism, $J_{5.5-10.5}$ (eq. (D.10)), results from the interaction between the 5.5 components and the 10.5 components. The $U_{10.5}$ component results from the interaction between the 5.5 components and the 8 components, which produces several terms in the $U_{10.5}$ equation. Most of the terms in the $U_{10.5}$ equation (4.13) produce no velocity jump. Only three terms,

$$Q^* U_8^{(20)}, \quad \left[V_{5.5}^{(11)} \left(U_8^{(02)} W_8^{02} \right) \right], \text{ and } \quad V_8^{(20)} Q_\eta^* ,$$

interact with the 5.5 components to produce the velocity jump. The interactions of these three terms with $V_{5.5}$ produce G_a (eq. (D.11a)); their interaction with Q_η produces G_b (eq. (D.11b)); and their interaction with Q produces G_c (eq. (D.11c)).

REFERENCES

Bodonyi, R.J. and Smith, F.T. 1981 The upper branch stability of the Blasius boundary layer, including non-parallel flow effects. Proc. R. Soc. Lond. A375, 65-92.

Corke, T.C. 1990 Effect of controlled resonant interaction and mode detuning on turbulent transition in boundary layers. To appear in Proceedings of the Third IUTAM Symposium on Laminar to Turbulent Transition, Toulouse, France, September 1989, (eds. R. Michell and D. Arnold), Springer.

Corke, T.C. and Mangano, R.A. 1987 Transition of a boundary layer: controlled fundamental-subharmonic interactions. Fluid Dynamics Center Rept. No. 87-1, Illinois Institute of Technology, Chicago, Illinois.

Corke, T.C. and Mangano, R.A. 1989 Resonant growth of three-dimensional modes in transitioning Blasius boundary layers. J. Fluid Mech. 209, 93-150.

Craik, A.D.D. 1971 Non-linear resonant instability in boundary layers. J. Fluid Mech. 50, 393-413.

Craik, A.D.D. 1986 Resonant interactions in shear flows. In Laminar-Turbulent Transition, (ed. V.V. Kozlov), Springer, 1-8.

Croswell, J.W. 1985 On the energetics of primary and secondary instabilities in plane poiseuille flow. MS Thesis, Virginia Polytechnic Institute State University, Blacksburg, VA.

DeVillers, J.M. 1975 Asymptotic solutions of the Orr-Sommerfeld equation, Phil. Trans. Roy. Soc. of London. A280, 271-316.

Drazin, P.G. and Reid, W.H. 1981 Hydrodynamic Stability. Cambridge University Press.

Eagles, P.M. 1969 Composite series in the Orr-Sommerfeld problem for symmetric channel flow. Q. J. Mech. Appl. Math. XXII, 129-182.

Fasel, H. 1990 Numerical simulation of instability and transition in boundary layer flows. To appear in Proceedings of the Third IUTAM Symposium on Laminar to Turbulent Transition, Toulouse, France, September 1989, (eds. R. Michell and D. Arnold), Springer.

Fraenkel, L.E. 1969 On the method of matched asymptotic expansions. Proc. Camb. Phil. Soc. 65, 209-231.

Goldstein, M.E. and Choi, W.W. 1989 Nonlinear evolution of interacting oblique waves on two-dimensional shear layers. J. Fluid Mech. 207, 97-120. (See also Corrigendum, J. Fluid Mech. 216, 659-663.)

Goldstein, M.E. and Durbin, P.A. 1986 Nonlinear critical layers eliminate the upper branch of spatially growing Tollmien-Schlichting waves. Phys. Fluids 29, 2344-2345.

Goldstein, M.E., Durbin, P.A., and Leib, S.J. 1987 Roll-up of vorticity in adverse-pressure-gradient boundary layers. J. Fluid Mech. 183, 325-342.

Goldstein, M.E. and Leib, S.J. 1988 Nonlinear roll-up of externally excited free shear layers. J. Fluid Mech. 191, 481-515.

Goldstein, M.E. and Hultgren, L.S. 1988 Nonlinear spatial evolution of an externally excited instability wave in a free shear layer. J. Fluid Mech. 197, 295-330.

Goldstein, M.E. and Leib, S.J. 1989 Nonlinear evolution of oblique waves on compressible shear layers. J. Fluid Mech. 207, 73-96.

Goldstein, M.E. and Wundrow, D.W. 1990 Spatial evolution of nonlinear acoustic mode instabilities on hypersonic boundary layers. J. Fluid Mech. 219, 585-607.

Goldstein, M.E. and Lee, S.S. 1991 The development of three-dimensional structures in adverse pressure gradient boundary layers. In preparation for J. Fluid Mech.

Graebel, W.P. 1966 On determination of the characteristic equations for the stability of parallel flow. J. Fluid Mech. 24, 497-508.
Haberman, R. 1972, Critical Layers in Parallel Shear Flows. Stud. Appl. Math. 51, 139-161.
Herbert, T. 1983 Subharmonic three-dimensional disturbances in unstable plane shear flows. AIAA Paper 83-1759.
Herbert, T. 1988 Secondary instability of boundary layers. In Annual Review of Fluid Mechanics, Vol. 20, (eds. J.L. Lumley, M. van Dyke, & H.L. Reed), Annual Reviews Inc., 487-526.
Huerre, P. 1987 On the Landau constant in mixing layers. Proc. R. Soc. Lond. A409, 369-381.
Kachanov, Yu.S., Kozlov, V.V., and Levchenko, V.Ya. 1978 Nonlinear development of a wave in a boundary layer. Fluid Dyn. 12, 383-390.
Kachanov, Yu.S. and Levchenko, V.Ya. 1984 The resonant interaction of disturbances at laminar-turbulent transition in a boundary layer. J. Fluid Mech. 138, 209-247.
Klebanoff, P.S. and Tidstrom, K.D. 1959 Evolution of amplified waves leading to transition in a boundary layer with zero pressure gradient. NASA TN D-195.
Klebanoff, P.S., Tidstrom, K.D., and Sargent, L.M. 1962 The three-dimensional nature of boundary-layer instability. J. Fluid Mech. 12, 1-34.
Kleiser, L. and Zang, T.A. 1991 Numerical simulation of transition in wall-bounded shear flows. Ann. Rev. Fluid Mech. 23, to appear.
Knapp, C.F. and Roache, P.J. 1968 A combined visual and hot wire anemometer investigation of boundary-layer transition. AIAA J. 6, 29-36.
Lin, C.C. 1955 The Theory of Hydrodynamic Stability. Cambridge University Press.
Maslowe, S. 1986 Critical layers in shear flows. Ann. Rev. Fluid Mech. 18, 405-432.
Miles, J.W. 1962 A note on the inviscid Orr-Sommerfeld equation. J. Fluid Mech. 13, 427-432.
Nayfeh, A. 1988 On subharmonic instability in boundary layers. In Forum on Unsteady Flow Separation; Proceedings of the First National Fluid Dynamics Congress, Cincinnati, Ohio, July 1988, (ed. K.H. Ghia), ASME, 103-117.
Raetz, G.S. 1959 A new theory of the cause of transition in fluid flows. NORAIR Rep. NOR-59-383, Hawthorne, California.
Reid, W.H. 1965 The stability of parallel flows. In Basic Developments in Fluid Dynamics, (ed. M. Holt), Academic Press, 249-308.
Robey, H.F. 1987 On the nature of oblique waves in boundary layer transition. In Turbulence Management and Laminarization. Proceedings IUTAM Symposium, Bangalore, India, (ed. H. Liepman and R. Narasimha), Springer-Verlag, 187-198.
Saric, W.S., Koslov, V.V., and Levchenko, V.Ya. 1984 Forced and unforced subharmonic resonance in boundary layer transition. AIAA Paper 84-0007.
Saric, W.S. and Thomas, A.S.W. 1984 Experiments on the subharmonic route to turbulence in boundary layers. In Turbulence and Chaotic Phenomena in Fluids, (ed. T. Tatsumi), North Holland, 117-122.
Saric, W.S. 1990 Boundary-layer stability and transition. In Numerical Ship Hydrodynamics, (ed. K.H. Mori), 23-33.
Schneider, S.P. 1989 Effects of controlled three-dimensional perturbations on boundary layer transition. Ph.D. Thesis, California Institute of Technology, Pasadena, California.
Schubauer, G.B. and Skramstad, H.K. 1947 Laminar boundary-layer oscillations and transition on a flat plate. J. Res. Natl. Bur. Stand. 38, 251-292.

Smith, F.T. and Stewart, P.A. 1987 The resonant-triad nonlinear interaction in boundary-layer transition. J. Fluid Mech. 179, 227-252.
Squire, H.B. 1933 On the stability for three-dimensional disturbances of viscous fluid flow between parallel walls. Proc. R. Soc. London A142, 621-628.
Stuart, J.T. 1986 Instability of flows and their transition to turbulence. Z. Flugwiss. Weltraumf. 10, 379-392.

Table 1. - Oblique waves' jump across the critical layer

J_0	Mean $\times \left(V_{5.5}\right)^{11} + V_8^{20}(5.5)^{-11}$ $= -i\,\frac{\pi}{4} A \frac{\bar{R}}{\lambda^2} - \frac{3}{4}\pi\bar{R}^2 A_o A^*$
J_1	$V_{5.5}^{(1-1)} \times (8)^{(02)} + (5.5)^{(-11)}(8)^{20}$ $= V_{5.5}^{(1-1)}\left(U_8^{02}, W_8^{02}\right) + 0$ $= 0.845\ A^2A^* \frac{\bar{R}^{3.5}}{\sqrt{\lambda}}$
J_2	$(UW + UU)_{5.5\times 8}$ $= (5.5)^{(1-1)}(8)^{02} + (5.5)^{(-11)}(8)^{20}$ $= (5.5)^{(1-1)}W_8^{02} + 0 + (5.5)^{(-11)}U_8^{20} + 0$ $= -5.39i\ A^2A^* \frac{\bar{R}^{3.5}}{\sqrt{\lambda}} + 0.21\ A^2A^* \frac{\bar{R}^{3.5}}{\sqrt{\lambda}}$
J_3	$U_{5.5}V_8$ $= U_{5.5}^{(1-1)}V_8^{02} + U_{5.5}^{(-11)}V_8^{20}$ $= -11.45\ A^2A^* \frac{\bar{R}^{3.5}}{\sqrt{\lambda}}$

Tao.e 2. - Jump across the critical layer

(a) Resulting from mean flow 8-component interaction.

$$J_{M-8}$$

$$\downarrow$$

mean × (8)

$$\downarrow$$

$$\bar{U}V_8^{20} + \ldots$$

$$\downarrow$$

$$2\bar{c}\,\mu_c\bar{\alpha}\cos\theta\,\bar{c}A_o + 0$$

$$\downarrow$$

$$-\frac{\pi i}{8}\frac{\bar{R}}{\lambda^2}A_o$$

(b) Resulting from 8-component self-interactions.

$$J_{8-8}$$

$$V_{5.5}U_{5.5}$$

$$U_8^{00}(\sim AA^*) \qquad U_8^{(2-2)}(\sim A^2) \qquad U_8^{02}(\sim A^*A)$$

$$\times \qquad\qquad \times$$

$$\text{linear}\left(V_8^{20} \sim A_o\right)$$

$$J_{8-8} = -\frac{2\pi\cos\theta}{\lambda^2\bar{c}^3h^2}\frac{\bar{\beta}}{\bar{\alpha}}\left[A_oAA^*\,h^{1/3}I_{8-1} + 2\frac{A^3A^*}{\lambda\bar{c}h^{1/3}}\frac{\bar{\beta}^2}{\bar{\alpha}^2}I_{8-8}\right]$$

Table 2. - Concluded.

(c) Resulting from 5.5-10.5 interactions.

	$J_{5.5-10.5}$
=	$G_a + G_b + G_c$
G_a:	$V_{5.5}^{(11)} U_{10.5}^{(11)}$ $V_{5.5}^{(11)}(\sim A)\left[Q^* U_8^{20}(\sim A^* A^2),\ V_{5.5}^{(11)} U_8^{(02)}(\sim A^* A^2),\ V_8^{20} Q_\eta^*(\sim A_o A^*),\ \ldots\right]$
G_a =	$-\pi \frac{\bar{\beta}}{\bar{\alpha}} \frac{A^3 A^*}{\lambda^3 \bar{c}^4} \frac{1}{h^{7/3}} \left(\frac{2}{3} \frac{\bar{\beta}^2}{\bar{\alpha}^2} \sin\theta\, T_{a1} - 3 \frac{\bar{\gamma}}{\bar{\alpha}} T_{a5}\right) + \pi \frac{\bar{\beta}^2}{\bar{\alpha}\bar{\gamma}} \frac{A_o A^* A}{\lambda^2 \bar{c}^3 h^{5/3}} T_{a4}$
G_b:	$Q_\eta(U^{(11)}, W^{(11)})$ $A\left[Q^* U^{20}(\sim A^* A^2),\ V_{5.5}^{(11)}\left(U_8^{(02)} + W_8^{02}\right)(\sim A^* A^2),\ V_8^{20} Q_\eta^*(\sim A_o A^*),\ \ldots\right]$
G_b =	$6\pi \left(\frac{\bar{\beta}}{\bar{\alpha}}\right)^2 \frac{\sin\theta}{\lambda^3 \bar{c}^4} \frac{A^* A^3}{h^{7/3}} \left[2 \frac{\bar{\beta}^2}{\bar{\alpha}^2} \sin\theta\, T_{b1} + \frac{\bar{\gamma}}{\bar{\alpha}} (3\cos\theta - \sin\theta) T_{b5} + 0\right]$
G_c:	$Q(U_\eta^{(11)}, W_\eta^{(11)})$ $A\left[Q^* U^{20}(\sim A^* A^2),\ V_{5.5}^{(11)}\left(U_8^{(02)} + W_8^{02}\right)(\sim A^* A^2),\ V_8^{20} Q_\eta^*(\sim A_o A^*),\ \ldots\right]$
G_c =	$-\frac{4\pi\bar{\beta}^2}{\bar{\alpha}^2} \frac{A^* A^3}{\lambda^3 \bar{c}^4 h^{7/3}} \left[\frac{3\bar{\beta}^2}{\bar{\alpha}^2} \sin^2\theta\, T_{c1} + \frac{\bar{\gamma}}{\bar{\alpha}} \sin\theta(6\cos\theta - \sin\theta) T_{5c}\right.$ $\left. - \frac{4\pi\bar{\beta}}{\bar{\alpha}} \frac{A_o A A^* \sin^3\theta}{\lambda^2 \bar{c}^3 h^{5/3}} T_{4c}\right]$

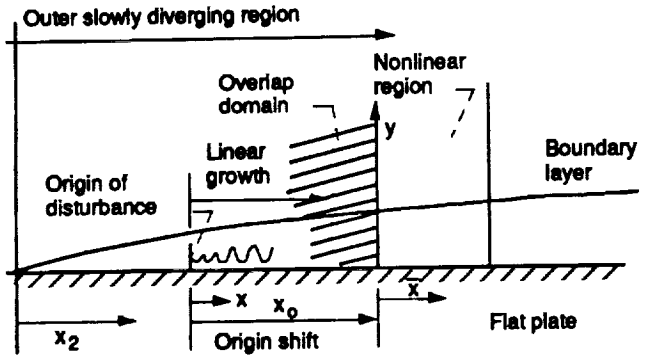

(a) Flow.

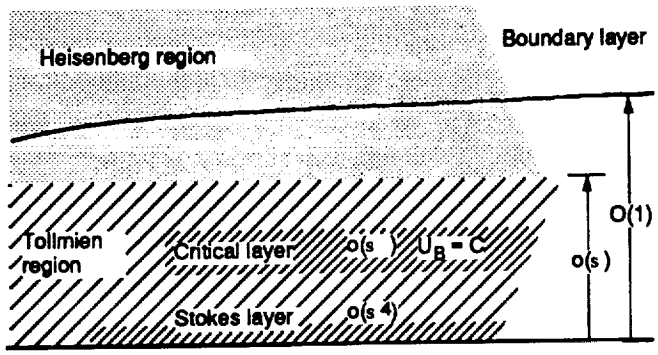

(b) Stability

Figure 1.—Structure.

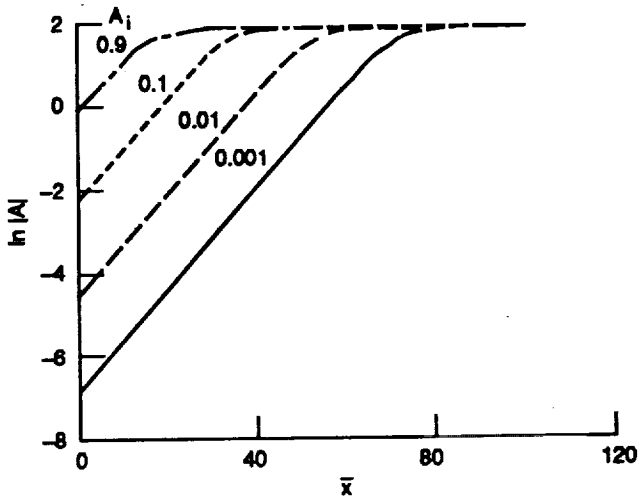

Figure 2.—Amplitude of the oblique waves under variable initial levels, in the absence of the plane waves. The oblique waves' self-interaction leads to their saturation. Note that the saturation level of the oblique waves is independent of the intial amplitude.

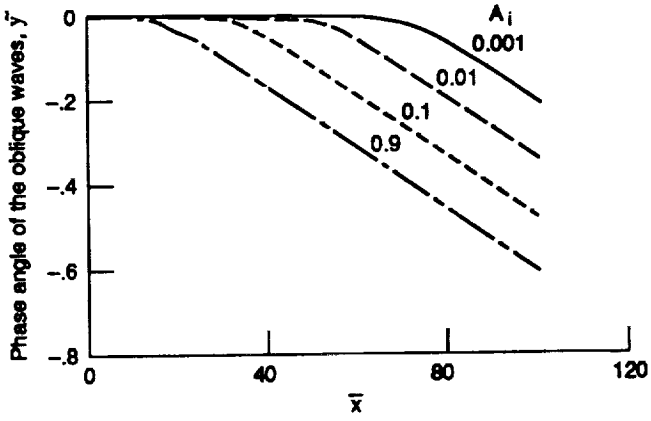

Figure 3.—The phase angle of the oblique waves' amplitude in the absence of the plane wave. Nonlinearity causes the initially real amplitude to become complex.

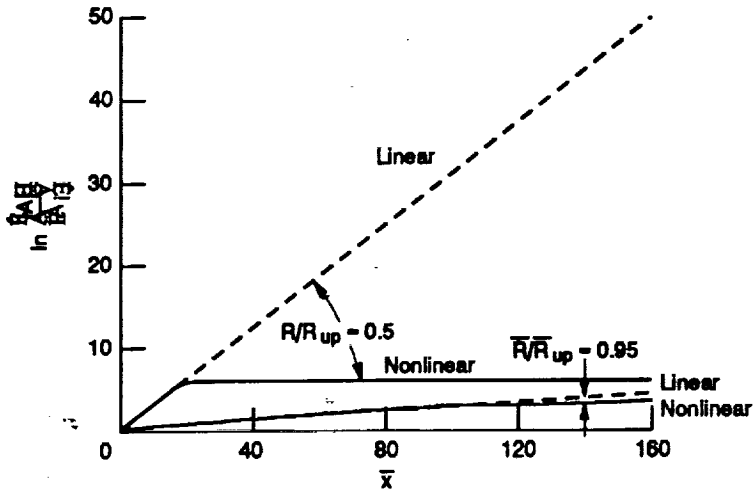

Figure 4.—The effect of the scaled Reynolds number on the oblique waves' nonlinear development in the absence of the plane wave (A_1 = 0.1). The saturation level of the oblique wave slowly decreased with the Reynolds number.

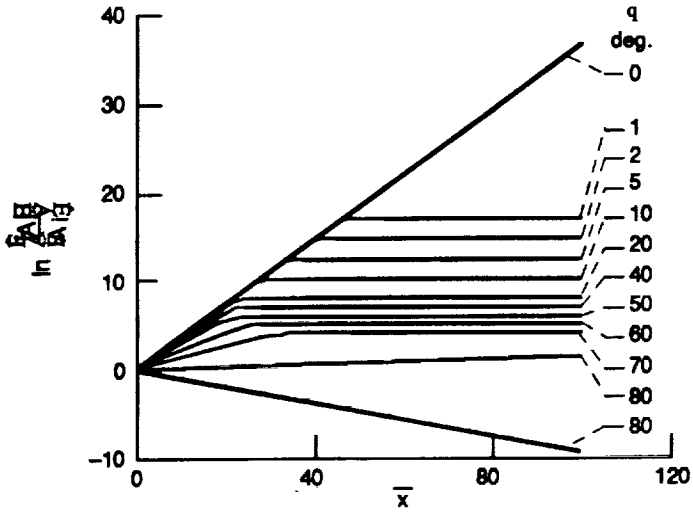

Figure 5.—The effect of obliqueness angle, q, on the nonlinear development of the oblique waves in the absence of the plane wave (A_1 = 0.1).

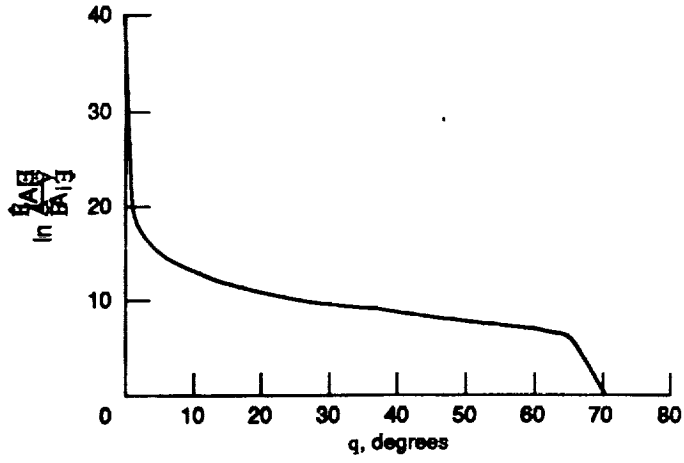

Figure 6.—The effect of obliqueness angle, q, on the amplitude of the oblique waves at $\bar{x}$ = 100 (A_1 = 0.1). Note the sharp drop at 0° < q <5°.

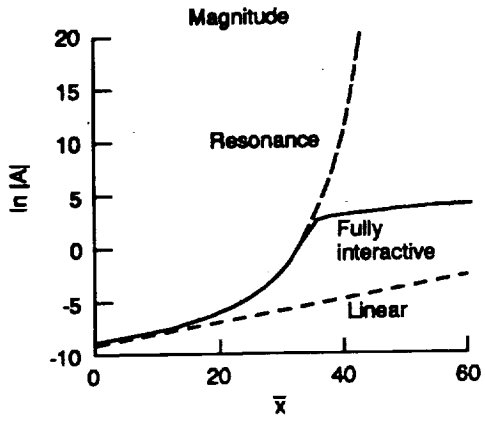

(a) Magnitude.

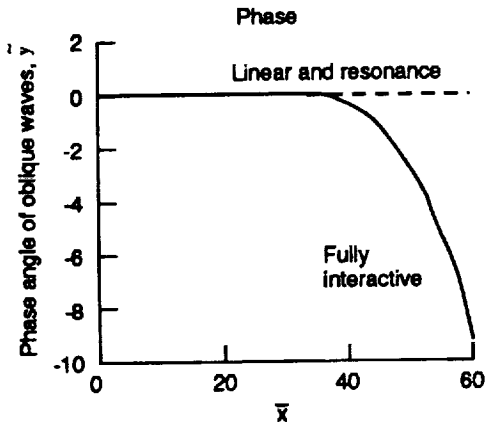

(b) Phase.

Figure 7.—Oblique wave development.

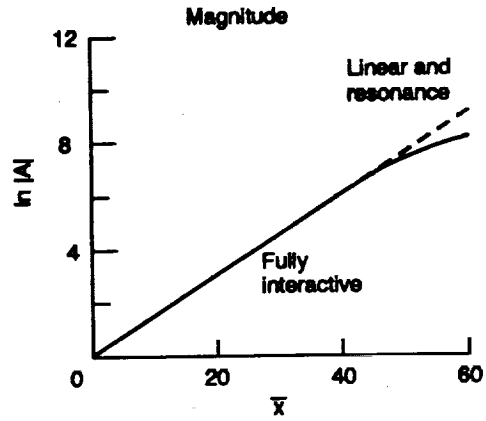

(a) Magnitude.

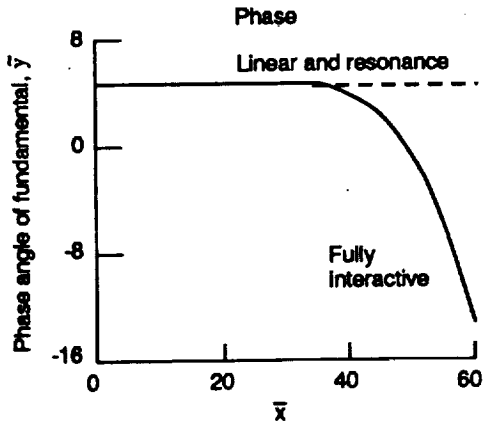

(b) Phase.

Figure 8.— The fully interactive development of the plane wave.

REPORT DOCUMENTATION PAGE

Form Approved
OMB No. 0704-0188

1. AGENCY USE ONLY (*Leave blank*)	2. REPORT DATE	3. REPORT TYPE AND DATES COVERED
	September 1991	Technical Memorandum

4. TITLE AND SUBTITLE
Resonant Triad in Boundary-Layer Stability
Part I. Fully Nonlinear Interaction

5. FUNDING NUMBERS
WU-505-62-21

6. AUTHOR(S)
Reda R. Mankbadi

7. PERFORMING ORGANIZATION NAME(S) AND ADDRESS(ES)
National Aeronautics and Space Administration
Lewis Research Center
Cleveland, Ohio 44135-3191

8. PERFORMING ORGANIZATION REPORT NUMBER
E-5233-1

9. SPONSORING/MONITORING AGENCY NAMES(S) AND ADDRESS(ES)
National Aeronautics and Space Administration
Washington, D.C. 20546-0001

10. SPONSORING/MONITORING AGENCY REPORT NUMBER
NASA TM-105208

11. SUPPLEMENTARY NOTES
Responsible person, Reda R. Mankbadi, (216) 433-8569.

12a. DISTRIBUTION/AVAILABILITY STATEMENT
Unclassified-Unlimited
Subject Category 34

12b. DISTRIBUTION CODE

13. ABSTRACT (*Maximum 200 words*)

A first-principles theory is developed to study the nonlinear spatial evolution of a near-resonance triad of instability waves in boundary-layer transition. This triad consists of a plane wave at fundamental frequency and a pair of symmetrical, oblique waves at the subharmonic frequency. A low-frequency, high-Reynolds-number asymptotic scaling leads to a distinct critical layer where nonlinearity first becomes important; the development of the triad's waves is determined by the critical layer's nonlinear, viscous dynamics. The resulting theory is fully nonlinear in that all nonlinearly generated oscillatory and nonoscillatory components are accounted for. The presence of the plane wave initially causes exponential-of-exponential growth of the oblique waves. However, the plane wave continues to follow the linear theory, even when the oblique waves' amplitude attains the same order of magnitude as that of the plane wave. A fully interactive stage then comes into effect when the oblique waves exceed a certain level compared to that of the plane wave. The oblique waves react back on the fundamental, slowing its growth rate. The oblique waves' saturation results from their self-interaction—a mechanism that does not require the presence of the plane wave. The oblique waves' saturation level is independent of their initial level but decreases as the obliqueness angle increases. Part II of this study will present results for the composite solution and comparisons with observations. Novel features of the phenomena will be described, and new interpretations of the experimental data will be given therein.

14. SUBJECT TERMS	15. NUMBER OF PAGES
Stability; Transition; Boundary-layers	56
	16. PRICE CODE A04

17. SECURITY CLASSIFICATION OF REPORT	18. SECURITY CLASSIFICATION OF THIS PAGE	19. SECURITY CLASSIFICATION OF ABSTRACT	20. LIMITATION OF ABSTRACT
Unclassified	Unclassified	Unclassified	